A disease-linked ULBP6 polymorphism inhibits NKG2D-mediated target cell killing by enhancing the stability of NKG2D ligand binding

Zuo, Jianmin; Willcox, Carrie; Mohammed, Fiyaz; Davey, Martin; Hunter, Stuart; Khan, Kabir; Antoun , Ayman ; Katakia, Poonam; Croudace, Joanne; Inman, Charlotte; Parry, Helen; Briggs, David; Malladi, Ram; Willcox, Benjamin; Moss, Paul

DOI:
10.1126/scisignal.aai8904

A disease-linked *ULBP6* polymorphism inhibits NKG2D-mediated target cell killing by enhancing the stability of NKG2D-ligand binding

Jianmin Zuo,[1*] Carrie R. Willcox,[1*] Fiyaz Mohammed,[1*] Martin Davey,[1] Stuart Hunter,[1] Kabir Khan,[1] Ayman Antoun,[2] Poonam Katakia,[1] Joanne Croudace,[1] Charlotte Inman,[1] Helen Parry,[1,4] David Briggs,[3] Ram Malladi,[1,4] Benjamin E. Willcox,[1*†] Paul Moss[1,4*†]

[1]Cancer Immunology and Immunotherapy Centre, Institute of Immunology and Immunotherapy, University of Birmingham, Vincent Drive, Edgbaston, Birmingham, B15 2TT, UK. [2]School of Pharmacy, Faculty of Sciences and Engineering, University of Wolverhampton, WV1 1LY, UK. [3]National Health Service Blood and Transplant, Birmingham, B15 2SG, UK. [4]Department of Haematology, University Hospital Birmingham, B15 2TH, Birmingham, UK.

[*]These authors contributed equally to this study.

[†]Corresponding author. Email: p.moss@bham.ac.uk (P.M.); b.willcox@bham.ac.uk (B.E.W.)

ABSTRACT

NKG2D (natural killer group 2, member D) is an activating receptor found on the surface of immune cells, including natural killer (NK) cells, which regulates innate and adaptive immunity through recognition of the stress-induced ligands ULBP1 to ULBP6 and MICA/B. Similar to class I human leukocyte antigen (HLA), these NKG2D ligands possess a major histocompatibility complex (MHC)-like fold and exhibit pronounced polymorphism, which influences human disease susceptibility. However, whereas class I HLA polymorphisms occur predominantly in the α1α2 groove and affect antigen binding, the effects of most NKG2D ligand polymorphisms are unclear. Here, we studied the molecular and functional consequences of the two major alleles of *ULBP6*, the most polymorphic *ULBP* gene, which are associated with autoimmunity and relapse after stem cell transplantation. Surface plasmon resonance and crystallography studies revealed that the arginine-to-leucine polymorphism within ULBP0602 affected the NKG2D-ULBP6 interaction by generating an energetic hotspot. This resulted in an NKG2D-ULBP0602 affinity of 15.5 nM, which is 10- to 1000-fold greater than the affinities of other ULBP-NKG2D interactions and which limited NKG2D-mediated activation. In addition, soluble ULBP0602 exhibited high-affinity

competitive binding for NKG2D and partially suppressed NKG2D-mediated activation of NK cells by other NKG2D ligands. These effects resulted in a decrease in a range of NKG2D-mediated effector functions. Our results reveal that *ULBP* polymorphisms affect the strength of human lymphocyte responses to cellular stress signals, and may offer opportunities for therapeutic intervention.

INTRODUCTION

NKG2D is a major activating receptor on cytotoxic immune cells and plays an important role in innate immunity and stress surveillance. Conserved between mice and humans, NKG2D is found on a range of cytotoxic immune cells, including natural killer (NK) cells, γδ T cells, NKT cells, and αβ T cell subsets (*1*). A key feature of NKG2D is its interaction with many different NKG2D ligands on the surface of target cells. In humans, the main NKG2D ligands are the MICA/B and the ULBP proteins, whereas in mice, they consist of the RAET1, MULT-1, and H60 proteins (*2-5*). The amounts of NKG2D ligands at the cell surface increase during times of cellular stress, such as during viral infection (for example, with cytomegalovirus) (*6*) and tumorigenesis (*7-10*). Tumor cells and viruses evoke a range of mechanisms to evade recognition by NKG2D (*5*, *11-13*), highlighting the importance of this system of "lymphoid stress surveillance." NKG2D ligands are also found on dendritic cells and myeloid cell subsets (*14-16*), which suggests a potentially important influence of the NKG2D-ligands pathway on the link between innate and adaptive immunity.

NKG2D homodimers bind to NKG2D ligands in an interaction that is analogous to that seen in T cell receptor (TCR)–major histocompatibility complex (MHC) class I complexes (*17*). A striking feature of NKG2D ligand–encoding genes is their high rate of polymorphism (*18-21*), which mirrors the more extensive polymorphism observed within classical MHC-

encoding genes. Polymorphisms in the MHC-encoding genes are clustered mainly around the region encoding the antigen-binding groove, and they influence both the repertoire of bound peptides and binding by the T cell receptor (TCR) (*22*). Such polymorphisms are thought to have evolved in response to infectious challenge (*23*). NKG2D ligands are homologous to MHC molecules, and polymorphisms are focused within the *MICA/B* (*21*), *ULBP4*, and *ULBP6* genes (*18, 21, 24*). Interestingly, single nucleotide polymorphisms (SNPs) in NKG2D ligand–encoding genes are linked to human disease susceptibility and treatment outcome in several clinical disorders (*25-30*).

Most efforts to understand the functional importance of NKG2D ligand polymorphisms have focused on the valine–to-methionine dimorphism at position 129 of MICA, which is associated with overall survival after stem cell transplantation (*31*). This polymorphism in the region encoding the α2 domain of MICA is suggested to affect the avidity of NKG2D binding (*31, 32*) and the relative cell surface abundance of MICA (*33*). These and other studies have contributed to the concept that MICA polymorphisms tune the strength of the NKG2D-mediated response to specific MICA variants and have also revealed highly variable responses between individuals (*34*).

ULBP6 is one of the most recently discovered human NKG2D ligands and is highly polymorphic, with two haplotypes (*ULBP0601* and *ULBP0602*) together making up ~70% of the human population (*18, 19*). *ULBP6* polymorphisms are associated with diabetic nephropathy (*27*), alopecia areata (*29, 35*), and the clinical outcome after allogeneic hematopoietic stem cell transplantation (*25*). These studies highlight ULBP6 as an important immunoregulatory molecule and indicate the value of understanding the functional significance of the polymorphisms detected within the protein. We therefore undertook a

detailed analysis of the biophysical, structural, and functional importance of polymorphisms within *ULBP6*, focusing on the *ULBP0601/ULBP0602* dimorphism. We showed that a specific amino acid change within the ULBP0602 ectodomain had a substantial effect on the affinity of binding to NKG2D and resulted in an interaction with enhanced stability. This high-affinity interaction dampened the NKG2D-mediated activation of effector cells and reduced the magnitude of effector responses to target cells in all individuals tested. In addition, high-affinity soluble ULBP0602, which was released from the surface of ULBP0602-transfected cells, blocked the interaction between NKG2D and other ULBPs. Thus, *ULBP6* polymorphism acts as a critical regulator of human lymphoid stress surveillance and may represent an important immunotherapeutic target.

Results

ULBP6 is found on PBMCs and is increased in abundance in hematopoietic tumors

To understand the potential influence of allelic polymorphism on the function of ULBP6, we first studied the pattern of ULBP6 expression by hematopoietic cells (Fig. 1A). The currently used ULBP6-specific antibody also binds to ULBP2 and ULBP5, so we initially investigated the pattern of expression of the genes encoding these three ULBPs by quantitative reverse transcription polymerase chain reaction (qRT-PCR) analysis of primary CD4+ and CD8+ T cells, NK cells, B cells, and monocytes. The specificity of these qRT-PCR assays was first validated (fig. S1). HCT116 cells (a colorectal cancer cell line) were used as a positive control, whereas NKL, LCL, Jurkat, and HeLa cells were used as negative controls for ULBP6 expression (Fig. 1B).

Constitutive *ULBP6* transcription was relatively high in NK and B cells (median 106 and 86 copy numbers per 25 ng of cDNA reaction, respectively) but was lower in the other primary

cells (Fig. 1B). This amount of *ULBP6* mRNA in B cells and NK cells was several fold greater than that of *ULBP2* mRNA (median 7.1 and 18 copies per reaction, respectively), although high *ULBP2* transcription was observed in several cell lines (200 to 2000 copies per reaction) (Fig. 1B). *ULBP5* mRNA was undetectable in almost all primary cells and cell lines (Fig. 1B). Given this profile of expression within primary hematopoietic cells, we next determined the pattern of *ULBP6* expression in a range of primary hematological tumors (Fig. 1, C and D). Several hematological malignancies express at least one member of the NKG2D ligand family, although ULBP6 has not yet been studied in this regard (*36*). *ULBP6* transcription was substantially and specifically increased in tumor cells from patients with a range of lymphoid malignancies including chronic lymphocytic leukemia (CLL), acute lymphocytic leukemia, non-Hodgkin lymphoma, Hodgkin lymphoma, large granular lymphocytic lymphoma and PLPD. Median *ULBP6* mRNA abundance was approximately ~5 times higher than that observed in PBMCs from healthy control donors (Fig. 1C).

To investigate how *ULBP6* expression was altered in CLL, the most common subtype of leukemia, we compared transcriptional assays and anti-ULBP2/5/6 staining in healthy donor and primary CLL samples. Quantitative RT-PCR analysis demonstrated increases in *ULBP6* transcription, and to a lesser extent that of *ULBP2*, in PBMCs from CLL samples, whereas *ULBP5* mRNA was not detectable in either healthy donor samples or CLL samples (Fig. 1D). In addition, statistically significantly more staining by antibody against ULBP2, -5, and -6 was observed on primary CLL tumor cells than on healthy donor B cells (Fig. 1, E and F). This increase was relatively modest, consistent with studies on MICA and ULBPs 1 to 3, which have shown that NKG2D ligand expression is tightly controlled and that small alterations in NKG2D ligand abundance in response to stress stimuli can effectively modulate NKG2D-mediated responses (*37*). Finally, we assessed whether the *ULBP0601/02*

polymorphism influenced the transcription of *ULBP6* using sequence-specific polymorphism PCR as previously described (Fig. 1G) (*25*). No statistically significant difference in *ULBP6* expression was observed between the *ULBP0601* and *ULBP0602* genotypes within a cohort of hematological malignancy samples (Fig. 1G), suggesting that allelic variation does not influence transcriptional regulation of *ULBP6*. Together, these results support ULBP6 being a bona fide stress-induced NKG2D ligand that is increased in abundance during tumorigenesis, but suggest that the *ULBP6*01/02* polymorphism does not affect the stress-induced expression of *ULBP6*.

ULBP0602 has a high affinity for NKG2D

We next examined whether the *ULBP06*01/2* polymorphism influenced the molecular properties of the interaction of the protein with NKG2D. To assess this, we expressed recombinant ULBP6 with amino acids characteristic of the *01* and *02* haplotypes at the two polymorphic positions in the MHC-like ectodomain (hereafter termed ULBP0601, containing Arg^{106} and Ile^{147} and ULBP0602, containing Leu^{106} and Thr^{147}). The biophysical characteristics of the interaction of these proteins with NKG2D were then assessed with surface plasmon resonance (SPR) (Fig. 2). As expected, SPR detected the binding of NKG2D to the ligand. However, when the binding to ULBP0601, ULBP0602, and the other ULBPs were compared at similar immobilization values, disproportionately high binding responses and slow dissociation of NKG2D were observed for ULBP0602, indicating a particularly high affinity for this allelic form (Fig. 2A). It took more than two hours for NKG2D to completely dissociate from immobilized ULBP0602 when a flow rate of 10 µl/min was used. Equilibrium affinity analyses (Fig. 2B) determined an affinity of 15.5 nM for the ULBP0602-NKG2D interaction, which was more than 10-fold higher than the equivalent affinity of NKG2D for ULBP0601 (164.6 nM) and substantially greater than the affinities that we

determined for the other ULBP family members (fig. S2), which varied between approximately 300 nM and 35 μM (table S1). An affinity of ~1 μM was reported for the binding of MICA/B to NKG2D (*24*). Kinetic measurements confirmed an extremely slow dissociation for the ULBP0602 form, with a k_{off} of ~0.00125s^{-1} ($t_{1/2}$ of ~550 seconds) (Fig. 2C), substantially slower than the NKG2D-ULBP0601 interaction, which exhibited a k_{off} of ~0.022s^{-1} ($t_{1/2}$ of ~31 seconds) (Fig. 2C). These data indicate that the interaction between NKG2D and ULBP0602 and is much stronger than that with ULBP0601 and the other ULBP family members.

A structure of the NKG2D-ULBP6 complex was solved to 2.4 Å

To understand how ULBP0602 bound so strongly to NKG2D, and to determine the biophysical correlate of the UBP0601/2 polymorphism, we next determined the structure of the NKG2D-ULBP0602 interaction by X-ray crystallography to 2.4 Å (Fig. 3, A and B, and table S2). The core structure of ULBP0602, including the topology of its NKG2D-binding surface, closely resembles that of ULBP3 (Fig. 3C, overall rmsd: 2.1 Å), comprising two major helices atop an 8-stranded, antiparallel β-sheet, with interlocking hydrophobic residues generating a narrower cleft than that of the class I MHC molecule, which is unsuitable for binding antigenic peptides (Fig. 3D). Note that one third (23) of the nonconservative substitutions relative to ULBP3 map onto the MHC-like helical surface that serves as a primary contact site for NKG2D (fig. S3A).

Rigid body binding occurs within a conserved diagonal NKG2D interaction mode

The NKG2D-ULBP0602 interaction broadly resembles that from previously solved NKG2D-ligand structures, featuring the symmetric NKG2D homodimer bound to a monomeric ULBP0602 (Fig. 3A) through a diagonal mode similar to the NKG2D-ULBP3 (*38*) and

NKG2D-MICA (*39*) structures and akin to the TCR-pMHC interaction (Fig. 3E). The saddle-shaped NKG2D homodimer sits astride the ULBP6 helices, with NKG2D monomers A and B focused on the ULBP0602 α2 and α1 helices, respectively (Fig. 3A), resulting in a buried surface area (1855 $Å^2$) similar to that of NKG2D-ligand complexes (1930 to 2180 $Å^2$), and larger than those of the KIR-HLA (1560 $Å^2$) and TCR-pMHC (1700 to 1800 $Å^2$) interfaces. As noted for the NKG2D-ULBP3 interaction (*38*), three secondary structural elements from each NKG2D monomer stabilize the interface: the L1 loop (residues L150 to D152), the β5-β5' stirrup loop (residues M180 to S186), and the β6 strand (residues E195 to G200) (Fig. 3A). Notwithstanding relatively minor conformational differences in the stirrup loop of ULBP6-bound NKG2D relative to either unbound NKG2D (fig. S3B) or ULBP3-bound NKG2D (fig. S3C), no major conformational changes were observed, which is reflected by the low rmsd values for the NKG2D chains (0.8 to 0.9 Å).

Analysis of the NKG2D-ULBP0602 interface contacts indicated that the number of polar contacts used by ULBP0602 was similar to that of ULBP3 (Fig. 4A, fig. S4, and table S3). Note that the ULBP residues involved are not conserved within the family, either in position or identity (fig. S5, suggesting that family members use distinct combinations of interacting groups to bind to NKG2D (fig. S5). However, two charged residues, Glu^{96} and Asp^{189}, conserved between ULBP3 and ULBP0602, are positioned in the center of the interface and oriented diagonally with respect to the α1 and α2 helices (Fig. 4B). Glu^{96} and Asp^{189} are also conserved across the ULBP family (fig. S5) and, for both ULBP3 and ULBP0602, they mediate structurally conserved interactions to Lys^{150} and Lys^{197} in NKG2D, respectively (Fig. 4A and fig S5). It is tempting to speculate that they represent a conserved electrostatic orientation footprint, guiding NKG2D towards a diagonal mode of docking (Fig. 4B).

Hydrophobic interactions mediate the high affinity of the NKG2D-ULBP6 interaction

Hydrophobic contacts at the ULBP0602-NKG2D interface appear to play a defining role in determining the enhanced affinity of the ULBP0602 relative to that of ULBP0601 and explain why ULBP0602 has the strongest interaction with NKG2D. The previous NKG2D-ULBP3 structure highlighted a hydrophobic patch on each NKG2D subunit (comprising Tyr^{152}, Ile^{182}, Met^{184}, and Tyr^{199}), which interacts with ULBP3 around the C-terminal ends of the α2 helix (subunit A, "patch A") and the α1 helix (subunit B, "patch B") (*38*). Note that hydrophobic contacts to patch A are ~3-fold enhanced in ULBP0602-NKG2D interface compared to those in the ULBP3-NKG2D interface, which is mediated by the substitution of Thr^{181} and Met^{185} in ULBP3 with Met^{180} and Tyr^{184} at equivalent positions in ULBP6 (Fig. 4C and table S4). In addition, in ULBP6, Arg^{189} is replaced with Gly^{188}, which is likely to invoke less energetic penalties in terms of binding to Patch A as compared to ULBP3. Furthermore, the largely hydrophobic NKG2D Patch B forms fewer contacts (~25% reduced) with ULBP6 than with ULBP3 (table S3), which is determined largely by numerous contacts to ULBP3 Leu^{104}. However, as for Patch A, in ULBP3, the orientation of a charged Arg^{103} towards this hydrophobic region is likely to incur energetic penalties; in ULBP6 the equivalent residue is uncharged, favoring interaction.

The R106L polymorphism generates a hydrophobic hotspot that enhances the NKG2D-ULBP6 interaction

Examination of ULBP0601/02 allelic differences based on the NKG2D-ULBP6 structure indicated that the T147I change was unlikely to affect NKG2D binding, because this residue protrudes from the underside of the β-sheet (Fig. 4D). In contrast, the introduction of Leu^{106} in ULBP0602, which is located at the receptor-ligand interface (Fig. 4D), provides a clear rationale for enhanced affinity, because it inserts directly into the center of the hydrophobic

patch B of NKG2D, forming numerous nonpolar contacts with surrounding residues (Tyr^{152} Ile^{182}, Met^{184}, and Tyr^{199}) (Fig. 4, C and E, and table S4). In contrast, ULBP0601 has a charged and lengthy arginine at this position, and although its side chain can be accommodated without apparent steric clashes, its introduction within this predominantly hydrophobic environment is likely to be detrimental for NKG2D binding (Fig. 4F). To directly confirm the hypothesis that the 106 polymorphism was responsible for the higher affinity of ULBP0602 for NKG2D, relative to that of ULBP0601, we mutated both of the residues at the 147 and 106 positions of ULBP0602 to the residues found in ULBP0601. The ULBP0602-T147I mutant that retained Leu^{106} exhibited an affinity for NKG2D (13.4 nM) that was comparable to that of wild-type (WT) ULBP0602 (13.4 nM), whereas the affinity of the ULBP0602-L106R mutant (148.3 nM) was comparable to that of ULBP0601 (148.2 nM), indicating that the threonine-to-isoleucine mutation at position 147 had no effect on affinity (Fig. 4G). These results confirm the key role of polymorphism at position 106 in determining the high affinity of ULBP0602 for NKG2D.

ULBP0602 elicits less efficient NKG2D-dependent cytotoxicity than does ULBP0601

To assess the relative functional activities of the ULBP0601 and ULBP0602 proteins, we next tested their ability to elicit cytotoxicity in a range of $NKG2D^+$ lymphocytes, namely NK cells, αβ T cells, and γδ T cells. We therefore generated Chinese hamster ovary (CHO) cells expressing ULBP0601 and ULBP0602 variants for use as target cells (called CHO-ULBP0601 and CHO-ULBP0602, respectively) and used flow cytometric analysis to confirm that the cell lines had equivalent amounts of cell surface protein (Fig. 5A).

To assess NKG2D-mediated cytotoxicity within PBMCs, we used an established assay (*34*) that involved mixing equal numbers of either CFSE-labelled CHO-ULBP0601 or CHO-

ULBP0602 cells with mock-transfected CHO cells labelled with a 670-nm fluorescent dye (CHO-controls) in the presence or absence of activated PBMCs (see Materials and Methods). After coincubation with PBMCs, the ratio of CHO-ULBP0601 or CHO-ULBP0602 cells to CHO-controls was measured to determine relative cytotoxicity (Fig. 5B). Antibody-blocking experiments were used to confirm that such cytotoxicity was indeed NKG2D-dependent (Fig. 5B). Surprisingly, the ratio of CHO-ULBP0601 cells to CHO-controls was lower than the ratio of CHO-ULBP0602 cells to CHO-controls after co-incubation with PBMCs, indicating that the CHO-ULBP0601 cells elicited greater killing than did the CHO-ULBP0602 cells (Fig. 5B). To address donor-specific variation, we expanded the assay using PBMCs from 18 healthy donors. Although the overall level of killing observed varied substantially, for all donors, CHO-ULBP0601 cells elicited enhanced NKG2D-dependent killing relative to the CHO-ULBP0602 cells (mean killing of 42.6 and 30.4%, respectively; $P < 0.001$; Fig. 5C). This stronger NKG2D-dependent killing elicited by the CHO-ULBP0601 cells was further confirmed by a chromium-51 based assay, which highlighted more pronounced differences in cytotoxicity (>3-fold) at lower effector:target ratios (fig. S6). The cytotoxicity to Jurkat-ULBP0601 and Jurkat-ULBP0602 cells did not differ (fig. S7), which was possibly because of the expression of other NKG2D ligands on these cell lines.

These results suggest that the enhanced affinity of the NKG2D-ULBP0602 interaction led to the relatively less efficient cytotoxic activity of effector cells in response to ULBP0602-expressing cells compared to ULBP0601-expressing cells. To address this further, we next examined whether the exposure of NK cells to interactions with ULBP0602 could hinder the killing of CHO-0601 cells. Two combinations of CHO cell mixtures were established, consisting of a 1:1 mixture of either CHO-ULBP0601 and CHO-ULBP0602 cells or CHO-parental and CHO-ULBP0601 cells. The NK cell–mediated lysis of CHO-0601 cells was

markedly reduced in the presence of ULBP0602-expressing target cells (fig. S8), suggesting that engagement with ULBP602 indeed inhibited the ability of the NK cells to kill the surrounding target cells.

We next combined direct detection of target cell recognition by measurement of CD107a degranulation with co-staining of phenotypic markers to identify the nature of the responding $NKG2D^{+}$ cell populations. NK cells from healthy donor PBMCs showed substantial degranulation (20 to 40%) in response to CHO-ULBP6 cells compared to in response to parental CHO-control cells (Fig. 5D). In addition, the percentage of CD107a+ NK cells and the mean fluorescence intensity (MFI) of CD107a staining were consistently greater after incubation with CHO-ULBP0601 target cells than after incubation with CHO-ULBP0602 cells. Because the degree of NK cell activation can also be regulated by the abundance of NKG2D ligand, we next assessed how the relative surface expression of ULBP0601 or ULBP0602 on target cells influenced NK activation. CHO cells were transiently transfected with different amounts of plasmids encoding ULBP0601 or ULBP0602 (5, 10, or 20 μg per 5×10^{6} cells) which led to differential cell surface protein expression, although the amounts of ULBP0601 and ULBP0602 were comparable for a given amount of plasmid (fig. S9A). These CHO cells were then co-cultured with primary NK cells, and NK cell activation was determined by measuring the intensity of CD107a staining. The intensity of CD107a staining was maximal upon co-incubation with either the ULBP0601 or ULBP0602 transfectants that received 10 μg of plasmid (fig. S9B). However, NK cell activation in response to co-incubation with cells transfected with 10 or 20 μg of plasmid was markedly for the ULBP0601 target cells as compared to the ULBP0602 target cells (fig. S9C).

Soluble NKG2D ligands are able to block the engagement of NKG2D with its ligands (*40*); thus, we generated and purified soluble ULBP0601 and ULBP0602 proteins. These were initially incubated with NK cells for 16 hours before the pattern of NKG2D expression was assessed by flow cytometry. Soluble ULBP0602 blocked the binding of NKG2D-specific antibody to NKG2D, but this effect was not observed when the lower affinity ULBP0601 protein was used in concentrations up to 10 µg/ml. (Fig. 6, A and B). To determine whether this blockade had the potential to modulate NK cell function, we assessed the pattern of NK cell activation in response to K562 cells in the presence or absence of soluble ULBP6. We found that both ULBP0601 and ULBP0602 partially blocked NK cell activation by K562 cells and that this effect was more substantial after incubation with ULBP0602 than with ULBP0601 (Fig. 6C). We therefore investigated whether soluble ULBP0601 or ULBP0602 are released into the conditioned medium of CHO transfectants and whether this contributed to the observed pattern of differential cellular activation. Low amounts of soluble ULBP0601 and ULBP0602 were indeed released into the culture medium after 12 hours of incubation, and typically reached comparable concentrations (~400 pg/ml) for both variants (Fig. 6 D). To assess whether soluble ULBP6 blocked the binding of other soluble ligands to NKG2D, we incubated the NKL cell line with ULBP2-Fc protein in the presence or absence of conditioned medium from the ULBP06-transfectants. The extent of ULBP2-Fc binding to the NKL cells was measured by flow cytometric analysis of the binding of an anti-Fc antibody. Conditioned media from both CHO-ULBP0601 and CHO-ULBP0602 transfectants partially blocked the binding of ULBP2-Fc to the NKL cell line, although this effect was more pronounced with CHO-ULBP0602 (37% inhibition compared to 14% by ULBP0601) (Fig. 6E).

Next, we tested the effect of ULBP6 polymorphism on NKG2D-dependent γδ and αβ T cell responses. Human peripheral blood Vγ9Vδ2 T cells proliferated in response to (E)-4-Hydroxy-3-methyl-but-2-enyl pyrophosphate (HMBPP), expressed high amounts of NKG2D (Fig. 7A), and demonstrated enhanced killing of CHO-ULBP0601 cells compared to CHO-ULBP0602 cells, indicating differential co-stimulation of γδ T cells responding to HMB-PP by ULBP06 variants (Fig. 7, B and C). In addition, $NKG2D^+$ αβ cytotoxic T cell clones (Fig. 7D) specific for EBV epitopes restricted by HLA-B7 displayed substantially enhanced production of IFN-γ in response to cognate antigen-pulsed Jurkat cells (which naturally express HLA-B7) transfected with plasmid encoding ULBP0601 (JKT-ULBP0601 cells) compared to those expressing ULBP0602 (JKT-ULBP0602 cells) (Fig. 7E), suggesting that *ULBP6* polymorphism markedly influences the efficiency of HLA-restricted T cell costimulation (Fig. 7F). In summary, polymorphisms in *ULBP6* substantially influenced the strength of NKG2D-dependent effector responses, with the lower-affinity ULBP0601 allotype being more potent than the higher-affinity ULBP0602 allotype.

The functional potency of ULBP0602 is limited by polymorphism at position 106

We next tested whether altering the affinity of ULBP6 affected its potential to elicit NK cell cytotoxicity. After confirming NKG2D expression on the NKL cell line (Fig. 8A), NKL-mediated cytotoxicity was assessed in the presence of a range of different target cell lines. These included CHO-ULBP0601 and CHO-ULBP0602 cells (Fig. 8B), as well as CHO-ULBP0602-L106R and CHO-ULBP602-T147I cells, which carried single amino acid changes at positions 106 and 147 within ULBP0602 (Fig. 8C). Competitive cytotoxic assays were then performed and, as expected, NKL cells showed dose-dependent specific killing of CHO-ULBP0601 and CHO-ULBP0602 cells, with the CHO-ULBP0601 cells eliciting greater cytotoxicity than that elicited by the CHO-ULBP0602 cells (Fig. 8B). The CHO-

ULBP0602-L106R transfectant, which expressed a mutant of ULBP0602 with an NKG2D affinity matching that of ULBP0601, elicited greater cytotoxicity than did CHO-ULBP0602 cells, and indeed was comparable to CHO-ULBP0601 cells (Fig. 8D, left). In contrast, CHO-ULBP602-T147I cells elicited comparable cytotoxic responses to those elicited by CHO-ULBP0602 cells (Fig. 8D, right), suggesting that the Leu^{106} SNP in ULBP0602 is responsible for both its high affinity for NKG2D and its limited functional potency relative to that of ULBP0601 (Fig. 8E).

Differential NKG2D-ULBP6 affinities affect NKG2D signaling and receptor downregulation

To understand how differential NKG2D-ULBP6 affinities could lead to altered effector cell responses, we assessed NKG2D downregulation (decreased cell surface expression), a surrogate indicator of receptor stimulation. After 1 hour of co-culture with CHO-ULBP0601 cells, NKL cells showed ~80% downregulation of cell surface NKG2D (Fig. 8F). In contrast, co-culture with CHO-ULBP0602 cells resulted in substantially less receptor downregulation (Fig. 8F), and this difference persisted throughout the 16-hour time course. This finding reveals that ULBP0601 induced more efficient NKG2D downregulation than did the higher affinity ligand ULBP0602, which is suggestive of differential signaling. To address this, we assessed calcium flux after the engagement of NKG2D with either ULBP601 or ULBP0602. NKL cells loaded with Calcium Sensor Dye were acquired by flow cytometry before and after exposure to CHO-ULBP0601 or CHO-ULBP0602 cells. Relative to their basal calcium concentration, NKL cells co-incubated with CHO-ULBP0601 cells had statistically significantly increased free intracellular calcium concentrations compared to those in NKL cells co-incubated with CHO-ULBP0602 cells (Fig. 8G).

DISCUSSION

NKG2D ligands are thought to play a central role in the immunological control of infection and malignant disease. Notably, both ULBP and MIC proteins exhibit considerable polymorphism. However, the functional importance of these polymorphisms, the factors that have driven their selection, and how they might influence relevant disease mechanisms has remained largely unclear. We chose to focus on *ULBP6* because this is the most polymorphic gene within the ULBP family, and SNPs within *ULBP6* are associated with several clinical disorders (*25*, *27*, *29*).

We showed that the two common allelic variants of ULBP6, ULBP0601 and ULBP0602 (*19*, *25*) elicited distinct NKG2D-dependent responses and exhibited profound differences in the affinity of NKG2D binding, which resulted in differential capacity to activate effector cells. Specifically, engagement with ULBP0601 elicited substantially enhanced NKG2D-dependent responses relative to those elicited by ULBP0602. Although the extents of the differences in effector responses elicited by ULBP0601 and ULBP0602 were relatively modest (typically ≤30%, but up to ~3-fold in chromium-release assays), these differences were observed in all $NKG2D^+$ effector subsets (NK cells, as well as αβ and γδ T cells), in relation to a range of different effector responses (cytotoxicity, cytokine production) and consistently across every individual tested. Thus, this common NKG2D ligand dimorphism can modulate the strength of NKG2D-mediated stress responses. We also outlined a previously uncharacterized molecular mechanism whereby this occurs, namely through a key polymorphic amino acid change at position 106 (Arg→Leu) which affects the strength and stability of the NKG2D-ULBP6 interaction. Previous studies on MICA have highlighted high inter-individual variation in NKG2D-mediated responses (*34*), and the varying magnitude of the NK cell response that we observed between individuals is consistent with this. However, the hierarchy

of responses to different polymorphic MICA variants was also found to vary between individuals (*34*). In contrast, the existence of a dominant hierarchy of functional responses to the ULBP6 dimorphic variants conserved in all individuals tested (ULBP0601>ULBP0602) hints at new mechanisms underpinning regulation of NKG2D-mediated responses.

Previously, *ULBP6* polymorphism was linked to diabetic nephropathy (*27*), autoimmune alopecia (*29*), and differential clinical outcome following SCT (*25*). Although the precise mechanisms that operate in each clinical scenario are unclear, we suggest that variability in the strength of NKG2D-mediated cellular responses contributes to such susceptibilities. Interestingly, despite eliciting stronger effector responses compared to those elicited by ULBP0602, the ULBP0601 variant is associated with reduced survival after SCT (*25*), perhaps suggesting that enhanced NK cell–mediated reduction in tumor antigen availability or elimination of antigen-presenting cells (APCs) (*41-44*) or T cells (*45, 46*) suppresses the subsequent development of alloreactive T cell immunity. Note that ULBP0602 mediated reduced NKG2D-mediated responses when expressed at the cell surface and in soluble form was a more potent suppressor of such responses than was ULBP0601. Our observation of increased *ULBP6* expression in hematological tumor cells is consistent with the first model, and future studies may suggest novel immunotherapeutic strategies based on these concepts involving NKG2D-ULBP6–targeted immunomodulation after SCT and/or complementary vaccination or adoptive cell transfer approaches.

Alopecia areata (AA) is a T cell–driven autoimmune condition (*47, 48*) and a *ULBP6* SNP (rs9479482) is strongly associated with this condition, with the highest odds ratio of any locus outside the MHC (*29*, *35*). Consistent with this, $NKG2D^+$ T cells are critical mediators in initiating AA (*48*) and ULBP3 abundance is increased in hair follicles during active

disease (*29*). Another *ULBP6* SNP (rs1543547) showed the strongest linkage among >11,000 SNPs analyzed for association with diabetic nephropathy, which is now a leading cause of renal failure and necessity of dialysis (*27*). Although previous studies have highlighted the important contribution of $NKG2D^+$ T cells to nephropathy, the pattern of expression of ULBP6 has not yet been examined (*49*). These genetic associations, combined with our finding that ULBP6 can act as an important costimulatory molecule for T cell recognition, support a role for pathogenic cytotoxic T cell responses in susceptible individuals and suggest that local expression of ULBP6 in the skin and kidney, respectively, may be of considerable clinical importance.

The molecular mechanisms whereby the *ULBP0601/02* polymorphism influences NKG2D-mediated responses are also of interest. The NKG2D-ULBP0602 structure revealed that, by inserting into a non-polar pocket in NKG2D, the R106L polymorphism contributes to a distinct interface featuring a double hydrophobic hotspot. This may explain why ULBP0602 has the highest affinity for NKG2D of all of the NKG2D ligands, with a value that is >10-fold higher than that of ULBP0601. This structure also sheds light on NKG2D recognition in general, where previous studies have invoked either "induced fit" or "rigid body adaptation" *(38, 39)* mechanisms to explain the remarkable ability of NKG2D to interact with eight relatively diverse ligands (ULBP1 to ULBP6, MICA, and MICAB). Notwithstanding relatively minimal conformational alterations in NKG2D upon ULBP6 engagement, our structural data indicate that ULBP6 and ULBP3 use very distinct molecular mechanisms of binding to NKG2D, which is consistent with rigid body adaptation (*39*). Moreover, our data reveal that underlying these diverse interaction profiles is a conserved electrostatic core comprising Glu^{96} and Asp^{189} on ULBP6, which interact with lysine residues in patch A and B on NKG2D, respectively. These two negatively charged residues are conserved across the

entire ULBP family, and their diagonal orientation most likely guides NKG2D to dock in its diagonal binding mode. Our data thus suggest that a conserved "electrostatic restriction" to NKG2D ligand underpins the degenerate recognition by NKG2D of its diverse ligands.

Our results also may explain how the substantial differences in affinity and kinetics in the interactions between NKG2D and ULBP0601 or ULBP0602 translate into differential functional effects. ULBP0602 exhibited a higher affinity than that of ULBP0601 for NKG2D, but engendered weaker NKG2D-mediated responses. One possibility is that the generation of soluble forms of ULBP06 underlies these functional differences. Consistent with this, we demonstrated that soluble recombinant ULBP0602 exhibited strong binding to NKG2D and had the potential to competitively inhibit NKG2D binding to alternative NKG2D ligands, leading to a greater relative suppression of NKG2D-mediated effector cell responses compared to ULBP0601. Indeed, this effect was observed to a modest extent with the use of conditioned medium from ULBP6-expressing transfected cell lines (Fig. 6, D and E), suggesting that cleavage of the ligand from the cell surface may play an important physiological role in vivo (*13, 40*). A second mechanism that may operate relates to the stable nature of the NKG2D-ULBP0602 interaction, which equates to a $t_{1/2}$ of ~550 s at 25°C, and is likely to limit serial triggering of NKG2D molecules at the surface of the effector cell. In contrast, the faster k_{off} for ULBP0601, equating to a $t_{1/2}$ of ~31 ss at 25°C, could elicit much more efficient serial triggering of NKG2D. Serial triggering of TCRs by pMHC molecules is required for TCR downregulation and the intracellular signaling events that lead to activation (*50, 51*). Indeed, the more efficient downregulation of NKG2D molecules elicited by ULBP0601 suggests that NKG2D serial triggering is likely to be the key discriminator between ULBP601 and ULBP602, translating differential binding kinetics into distinct functional responses. Consistent with this, enhanced calcium fluxes were observed after

NKG2D engagement by ULBP0601 relative to those stimulated by engagement with ULBP0602. Although it is unclear to what extent soluble ULBP6–mediated inhibition versus differential serial triggering effects drive the distinct biology of the two isoforms in vivo, our results highlight that, as for the TCR (*51*), the molecular properties of the NKG2D-ligand interaction play a key role in determining the efficacy of NKG2D-mediated effector cell responses.

Our findings raise questions about the evolutionary selection of the *ULBP0601* and *ULBP0602* alleles. Their coexistence at broadly equivalent and high frequencies, and their presence in diverse human populations, including Euro-Caucasoid, Afro-Caribbean, Indo-Asian (*18*), and an indigenous South American tribe (*52*), suggest that they arose in ancestral human populations and that the strength of NKG2D-mediated responses is the subject of strong and persistent evolutionary selection pressure. Interestingly, ULBP6 and ULBP4 are the only polymorphic ULBP molecules within the Kolla South American Indians and they exhibit linkage disequilibrium, indicating a potential selective advantage (*52*). One possibility is that different immunological challenges, such as protection against infection and immunological tolerance in pregnancy, may favor selection of these different forms. This potentially mirrors the evolution of *KIR* genes, whereby the balance of activating and inhibitory KIRs is thought to result from the action of similar environmental influences (*53*). NK cells within the decidua do indeed express ULBP (*54*), and as such polymorphism may influence reproductive success. Persistence of the *ULBP0601*/*02* dimorphism could also result from balancing selection, a phenomenon that is thought to have helped drive MHC allelic diversity because heterozygosity has an adaptive advantage over homozygosity. Conceivably, weaker NKG2D-mediated responses in *ULBP0602* homozygotes may compromise pathogen resistance, whereas *ULBP0601* homozygosity may impair

immunological tolerance. Consistent with *ULBP0601/02* heterozygotes displaying a distinct immunological phenotype, heterozygote survival after SCT is intermediate compared to that of *ULBP0601* and *ULBP0602* homozygotes (*25*). This observation suggests that therapeutically modulating the strength of NKG2D-mediated responses could be a viable route to improving patient outcomes both in SCT and other settings.

The considerable polymorphism within *ULBP6* and the association of these alleles, including *ULBP0601* and *ULBP0602*, with several clinical disorders suggests that this member of the NKG2D ligand family may represent an important therapeutic target (*25, 27, 29, 35*). However, rational interventions will require a more advanced understanding of the immunological mechanisms involved. This would include a better appreciation of how the strength of NKG2D-mediated responses affects the potency of alloreactive T cell responses after SCT (*25*). Similarly, an improved understanding of the regulation of ULBP6 expression in the context of autoimmunity (*27, 29, 35*) could shape future therapeutic ideas. Based on the results of such clinical studies, rational interventions that seek to modulate the strength of ULBP6-focussed effector responses within specific disorders may represent an important and unexpected source of novel immunotherapeutic approaches (*55*).

MATERIALS AND METHODS

Quantification of *ULBP* transcripts by qRT-PCR

Total RNA was isolated from whole PBMCs or purified lymphocyte populations with the QIAGEN RNeasy kit and was treated with DNase I (Turbo DNA-free kit; Ambion). Quantitative reverse-transcription polymerase chain reaction (qRT-PCR) assays for *ULBP2*, *ULBP5*, and *ULBP6* (*ULBP2*: Hs00607609-mH; *ULBP5*: Hs01584111-mH; *ULBP6*: Hs04194671-s1) were performed with TaqMan Gene Expression Assays (Applied

Biosystems), with β_2M (Hs00187842-m1) assayed for normalization. For absolute quantification of NKG2D ligand mRNAs, reference plasmids containing relevant ULBP or β_2M PCR target gene sequences were used to generate standard curves. $CD4^+$ T cells, $CD8^+$ T cells, NK cells, B cells, and monocytes were enriched by negative selection with magnetic beads, and purity was assessed by examining the combination of cell surface markers expressed ($CD4^+/CD3^+$, $CD8^+/CD3^+$, $CD56^+/CD16^+/CD3^-$, $CD20^+CD3^-$, and $CD14^+$, respectively).

Cell culture, cell lines, antibodies, and flow cytometric analysis

ULBP0601 and *ULBP0602* constructs were generated by site-directed mutagenesis and cDNAs were subcloned into the pcDNA5/FRT vector. The Flp-In-CHO and Flp-In-Jurkat cell lines were purchased from Invitrogen and maintained in Ham's F12 medium (Invitrogen) containing 10% fetal calf serum(FCS), penicillin (100IU/ml), streptomycin (100µg/ml), and Zeocin (100 µg/ml) or RPMI (Sigma) containing 10% FCS, Penicillin, Streptomycin, and Zeocin (100 µg/ml), respectively. The Flp-In-CHO cell line was transfected with ULBP-encoding plasmids with Lipofectamine LTX (Invitrogen), whereas Jurkat cell lines were transfected by electroporation, together with the pOG44 plasmid encoding the Flp-In recombinase. The stable transfectants were selected with Hygromycin (500 mg/ml). The NKL cell line was maintained in RPMI 1640, 10% FCS, and antibiotics with interleukin-2 (100 U/ml). PBMCs were isolated by Ficoll gradient. Blood samples from healthy donors were collected after informed consent. $CD4^+$ T cell, $CD8^+$ T cell, B cell, monocyte, and NK cell populations were separated with the EasySep human cell enrichment kit (Stemcell Technologies). Cell surface expression of ULBP6 or NKG2D on viable cells was determined by staining with APC-conjugated antibody against ULBP2/5/6 or isotype control antibody (R&D Systems) or with

APC-conjugated antibody against NKG2D or isotype control (BD Biosciences). Stained cells were analyzed on a BD Accuri C6 flow cytometer, and the data were processed with Flowjo software (Tree Star). APC conjugated anti-CD3, FITC-conjugated mouse anti CD107a, PE-conjugated mouse anti-CD56, and PE-conjugated mouse anti-CD8 antibodies were purchased from eBioscience. PE-conjugated anti TCR pan γδ was purchased from Beckman Coulter. Dye eFluor 670 and CFSE were purchased from eBioscience. For calcium flux analysis, NKL cells were harvested, washed, and loaded with Calcium Sensor Dye eFluor 514 (eBioscience) for 30 min at 37°C. NKL cells were then analzyed by flow cytometry (BD Accuri C6) for 1 min, removed for the addition of CHO-ULBP0601 or CHO-ULBP0602 cells, and immediately placed back on the flow cytometer for continued data acquisition.

NK cell cytotoxicity assays

The 1:1 mixture of ULBP0601 or ULBP0602 transfectants labeled with carboxyfluorescein diacetate succinimidyl ester (CFSE) and control transfected CHO cells labeled with Cell Proliferation Dye eFluor 670 were coincubated with effector cells (IFN-α–activated PBMCs) for 16 hours. After co-culture, the ratio of CFSE-negative cells (647 dye positive, control CHO cells) to CFSE-positive cells (ULBP0601 and ULBP0602 transfectant CHO cells) was calculated to determine the percentage of specific killing of each individual experiment. Lysis was calculated as follows: % specific lysis = 100 × {1 − [(control ratio)/(experimental ratio)]}. The control ratio refers to the ratio of CFSE-negative to CFSE-positive cells in the absence of effector cells, whereas the experimental ratio refers to the ratio of CFSE-negative to CFSE-positive cells in the presence of effector cells. Transfected CHO cell lines and IFN-α–activated PBMCs were co-cultured with FITC-conjugated anti-CD107a antibody for 5 hours. The cells were then washed and stained with combinations of APC-conjugated anti-CD3 and PE-conjugated anti-CD56 antibody to identify the NK cell population in the culture.

Stained cells were analyzed on a BD Accuri C6 flow cytometer, and the data were processed with Flowjo software (Tree Star).

T cell culture and effector cell assays

αβ T cell recognition was tested against Jurkat cell lines stably expressing ULBP0601 and ULBP0602, which were generated with the FRT-recombinase system as described earlier. For these assays, an HLA-B7–restricted, EBV-specific CD8+ T cell clone (specific for the BNRF1-derived epitope YPR and generated in our own lab) was used, and cultured in RPMI-1640 medium supplemented with 10% FCS, 30% supernatant from the IL-2-producing MLA-144 cell line, and 50U/ml recombinant IL-2. The capacity of the $CD8^+$ T cell clone to recognize target cells was measured by IFN-γ ELISA. The Jurkat-ULBP0601 cells and Jurkat-ULBP0602 cells were pulsed with serially diluted, synthetic YPR peptide and were used as targets in T cell assays with the YPR $CD8^+$ T cell clone. Briefly, 10^4 effector T cells were incubated for 18 hours at 37°C in microtest plate wells with 10^5 target cells, before assaying the supernatants for IFN-γ release by ELISA (Endogen) in accordance with the manufacturer's recommended protocol. Peripheral blood $V\delta2^+$ T cells were expanded from healthy donor PBMCs with 10 nM HMB-PP (Sigma) and 100 U/ml IL-2 (Miltenyi) for 14 days, and purified by magnetic bead isolation (Miltenyi) by selecting for TCR $V\delta2^+$ cells (123R3, Miltenyi). For γδ T cell killing assays, parental CHO cells (eFlour670-labelled) and CHO cells stably expressing either ULBP0601 or ULBP0602 (CFSE-labelled) were mixed 1:1 and co-cultured with the expanded purified $V\delta2^+$ T cells at various effector-to-target ratios (E:T) in the presence of medium or 1 nM HMB-PP and 40 U/ml IL-2 for 18 hours. Specific killing of CHO cells was monitored by staining with the amine reactive dead cell marker, Zombie Aqua (Biolegend).

Shedding of ULBP6 from CHO-ULBP6 cells and blocking of NKG2D ligand binding

The culture medium from overnight (12-hour) culture of CHO-parental, CHO-ULBP0601, and CHO-ULBP0602 cells was harvested and analyzed with a Human ULBP-2 DuoSet ELISA kit (R&D system DY1298). The concentration of ULBP6 was calibrated according to the recommendation from the product datasheet: a sample containing 1.56 ng/mL of rhULBP-6 reads as 435 pg/mL (27.9% cross-reactivity). For the blocking of the NKG2D ligand binding assay, NKL cells were cultured with the conditioned medium from both cultures and then stained with ULBP2-Fc proteins, which was followed by incubation with APC-conjugated anti-human Fc and analysis by flow cytometry.

Surface plasmon resonance assays

SPR was perfomed at 25ºC on a BIAcore 3000 in HBS-EP essentially as described previously (*56*). For these experiments, recombinant NKG2D was expressed in *E. coli* and purified, and ULBP proteins were expressed in the *Drosophila* Expression System, with or without terminal His-tag/BirA biotinylation tags as appropriate. Equilibrium affinity measurements were conducted at 5 to 10 µl/min, and Kd values were obtained either by Scatchard plots or by non-linear curve fitting of the Langmuir binding isotherm [bound = C*max/(Kd + C), where C is the analyte concentration and max is the maximum binding response] to data using the Levenberg-Marquardt algorithm as implemented in Origin 2015 (OriginLab Corporation). Concentrations of NKG2D and ULBPs were calculated as described previously (*57*). For experiments comparing the interaction of NKG2D with ULBP0601 and ULBP060602, NKG2D was injected over streptavidin-coated CM5 surfaces on which biotinylated ULBP0601 or ULBP060602 complexes were immobilized. Streptavidin-coated surfaces left blank or coated with endothelial protein C receptor (EPCR) produced in the *Drosophila* expression system were used as negative controls. The Kd values for the

NKG2D-ULBP0601 and NKG2D-ULBP0602 interactions in this orientation were 164.6 nM +/- 46 and 15.5nM +/- 4.3, respectively (n = 14 and n = 10 measurements, respectively). Equilibrium affinity measurements conducted similarly in the opposite orientation confirmed similar affinities (136.5 nM and 11.2nM for the NKG2D-ULBP0601 and NKG2D-ULBP0602 interactions, respectively). For most other NKG2D-ULBP interaction measurements, ULBP molecules were injected over immobilized NKG2D molecules or *E. coli*–produced HLA-A2 refolded with the Wilms Tumour protein (WT1)-derived peptide (RMFPNAPYL). For analysis of the effects of mutations at positions 106 and 147 on NKG2D interaction (Fig. 4G), NKG2D was injected over ULBP0602, ULBP0602-T147I, ULBP0602-L106R, or a control protein. In a second, separate experiment, NKG2D was injected over ULBP0601, ULBP0602-T147I, ULBP0602-L106R, or a control protein. Fig. 4G includes data from the two closely matched interactions (ULBP0602 and ULBP0602-T147I surfaces from the first experiment; ULBP0601 and ULBP0602-L106R from the second), with control responses subtracted. Immobilization values were similar between ULBP0601 and ULBP0602-L106R (960 and 974 RU, respectively), but marginally higher for ULBP0602 than ULBP0602-T147I (1036 and 967 RU, respectively), which could explain the higher binding responses to the ULBP0602 surface. Kinetic measurements to determine NKG2D-ULBP6 dissociation rate constants were performed with NKG2D as the analyte, using a flow rate of 50 µl/min to minimize mass transport considerations. Dissociation data were fitted to single exponential decay curves using the Langmuir 1:1 dissociation model as implemented in BIAevaluation 4.1.1 (GE Healthcare), and conformed to single order kinetics.

Protein expression, purification, and crystallization

For structural studies, the ectodomain of human NKG2D (residues Asn^{80} to Val^{216}) and ULBP0602 (residues Asp^{29} to Pro^{207}) were both expressed in *E. coli* Rosetta cells as inclusion bodies and then reconstituted in vitro. To facilitate correct refolding of ULBP0602, C34, which does not contribute to the canonical ULBP family intramolecular disulfide bond formation, was mutated to serine with the Quickchange Kit (Stratgene). Analysis of the final NKG2D-ULBP0602 structure confirmed that the side chain at position 24 was entirely solvent-exposed. In brief, NKG2D or ULBP0602 were expressed from pET23a plasmids at 37°C, purified from inclusion bodies as described previously (*56*), and then solubilized in 6 M guanidine hydrochloride before undergoing renaturation. NKG2D and ULBP0602 were then renatured separately by dilution refolding, which was performed with a refolding buffer consisting of 0.5 M L-arginine, 2.5 mM oxidized glutathione, 5 mM reduced glutathione, 0.1 M PMSF, and 100 mM Tris (pH 8.0). Renaturated NKG2D and ULBP0602 were then independently purified on a Superdex 200 column. ULBP0602 protein was further purified by anion exchange with a Resource Q column before crystallization, in 20 mM Tris (pH 8), 5 mM NaCl, and eluted over a 1 M NaCl gradient. Purified ULBP0602 and NKG2D proteins were concentrated and mixed in a 1:1 molar ratio. Initial crystallization screening was performed using the hanging drop vapor diffusion method with the Mosquito nanolitre crystallisation robot (TTP LabTech). NKG2D-ULBP0602 complex crystals formed after 3 to 4 days at 24°C with the Pact screen (Molecular Dimensions) condition 26, which consisted of 0.1 M PCB buffer (pH 5) and 25% PEG 1500 at an overall protein concentration of 9.9 mg/ml.

Data collection, structure determination, and refinement

NKG2D-ULBP0602 complex crystals were mounted directly from the mother liquor and flash cooled in liquid nitrogen. X-ray diffraction data were collected to 2.4 Å resolution using

an in house MicroMax 007HF rotating anode Rigaku X-ray generator with a Saturn CCD detector. The NKG2D-ULBP0602 complex crystallized in the monoclinic space group C2, with one NKG2D-ULBP0602 complex per asymmetric unit, and unit cell parameters a = 82.3 Å, b = 82Å, c = 73.2 Å, and β = 106.5°. All data were processed with XDS (*58*), with the relevant statistics listed in table S2. The complex structure was solved by molecular replacement using MOLREP (*59*), with the NKG2D-ULBP3 complex as the search model [PDB code: 1KCG (*38*)]. Refinement was performed with CNS (*60*) and REFMAC5 (*61*) interspersed with rounds of model building using COOT(*62*). Electron density maps were well-defined, enabling all amino side chains to be built. The stereochemical and refinement parameters are listed in table S2. All calculations relating to model validation, model analysis, and structure comparisons were performed with PROCHECK (*63*), programs of the CCP4 suite and the Uppsala Software Factory (*64*). All non-glycine residues are found in the allowed regions of the Ramachandran plot. Models of ULBP family members 1, 2, 4, and 5 were generated with the ULBP0602 structure as the template with the PHYRE server (*65*). Electrostatic surface potential maps were calculated with DelPhi (*66*). Structural figures were generated with PyMOL.

Statistical analysis

For univariate analyses, where data did not follow a normal distribution, either Mann-Whitney U test (for unpaired data) or Wilcoxon matched-paired signed rank test (for paired data) were used. Where data followed a normal distribution, the data were analyzed by either paired or unpaired, two-tailed t-tests. Where there were multiple independent variables, they were categorized and then analyzed by either one- or two-way ANOVA with Bonferroni post-hoc testing. All analyses were performed with Prism version 6.0 (Graphpad software).

Supplementary Materials

REFERENCES AND NOTES

1. D. H. Raulet, S. Gasser, B. G. Gowen, W. Deng, H. Jung, Regulation of ligands for the NKG2D activating receptor. *Annual review of immunology* **31**, 413-441 (2013).
2. S. Bahram, H. Inoko, T. Shiina, M. Radosavljevic, MIC and other NKG2D ligands: from none to too many. *Current Opinion in Immunology* **17**, 505-509 (2005).
3. S. Bauer, V. Groh, J. Wu, A. Steinle, J. H. Phillips, L. L. Lanier, T. Spies, Activation of NK Cells and T Cells by NKG2D, a Receptor for Stress-Inducible MICA. *Science* **285**, 727-729 (1999).
4. A. Cerwenka, A. B. H. Bakker, T. McClanahan, J. Wagner, J. Wu, J. H. Phillips, L. L. Lanier, Retinoic Acid Early Inducible Genes Define a Ligand Family for the Activating NKG2D Receptor in Mice. *Immunity* **12**, 721-727 (2000).
5. D. Cosman, J. Mullberg, C. Sutherland, W. Chin, R. Armitage, W. Fanslow, M. Kubin, N. Chalupny, ULBPs, novel MHC class I-related molecules, bind to CMV glycoprotein UL16 and stimulate NK cytotoxicity through the NKG2D receptor. *Immunity* **14**, 123 - 133 (2001).
6. V. Groh, R. Rhinehart, J. Randolph-Habecker, M. S. Topp, S. R. Riddell, T. Spies, Costimulation of CD8alphabeta T cells by NKG2D via engagement by MIC induced on virus-infected cells. *Nat Immunol* **2**, 255-260 (2001).
7. S. Gonzalez, A. Lopez-Soto, B. Suarez-Alvarez, A. Lopez-Vazquez, C. Lopez-Larrea, NKG2D ligands: key targets of the immune response. *Trends in Immunology* **29**, 397-403 (2008).
8. V. Groh, R. Rhinehart, H. Secrist, S. Bauer, K. H. Grabstein, T. Spies, Broad tumor-associated expression and recognition by tumor-derived gamma delta T cells of MICA and MICB. *Proceedings of the National Academy of Sciences of the United States of America* **96**, 6879-6884 (1999).
9. N. Nausch, A. Cerwenka, NKG2D ligands in tumor immunity. *Oncogene* **27**, 5944-5958 (2008).
10. J. Strid, S. J. Roberts, R. B. Filler, J. M. Lewis, B. Y. Kwong, W. Schpero, D. H. Kaplan, A. C. Hayday, M. Girardi, Acute upregulation of an NKG2D ligand promotes rapid

reorganization of a local immune compartment with pleiotropic effects on carcinogenesis. *Nat Immunol* **9**, 146-154 (2008).
11. C. A. Fielding, R. Aicheler, R. J. Stanton, E. C. Y. Wang, S. Han, S. Seirafian, J. Davies, B. P. McSharry, M. P. Weekes, P. R. Antrobus, V. Prod'homme, F. P. Blanchet, D. Sugrue, S. Cuff, D. Roberts, A. J. Davison, P. J. Lehner, G. W. G. Wilkinson, P. Tomasec, Two Novel Human Cytomegalovirus NK Cell Evasion Functions Target MICA for Lysosomal Degradation. *PLoS Pathog* **10**, e1004058 (2014).
12. V. Groh, J. Wu, C. Yee, T. Spies, Tumour-derived soluble MIC ligands impair expression of NKG2D and T-cell activation. *Nature* **419**, 734-738 (2002).
13. M. Jinushi, M. Vanneman, N. C. Munshi, Y. T. Tai, R. H. Prabhala, J. Ritz, D. Neuberg, K. C. Anderson, D. R. Carrasco, G. Dranoff, MHC class I chain-related protein A antibodies and shedding are associated with the progression of multiple myeloma. *Proceedings of the National Academy of Sciences of the United States of America* **105**, 1285-1290 (2008).
14. T. Ebihara, H. Masuda, T. Akazawa, M. Shingai, H. Kikuta, T. Ariga, M. Matsumoto, T. Seya, Induction of NKG2D ligands on human dendritic cells by TLR ligand stimulation and RNA virus infection. *International Immunology* **19**, 1145-1155 (2007).
15. M. Jinushi, T. Takehara, T. Tatsumi, T. Kanto, V. Groh, T. Spies, T. Suzuki, T. Miyagi, N. Hayashi, Autocrine/Paracrine IL-15 That Is Required for Type I IFN-Mediated Dendritic Cell Expression of MHC Class I-Related Chain A and B Is Impaired in Hepatitis C Virus Infection. *The Journal of Immunology* **171**, 5423-5429 (2003).
16. D. Schrama, P. Terheyden, K. Otto, U. Kämmerer, E.-B. Bröcker, F. Lühder, D. Cosman, M. H. Andersen, J. C. Becker, Expression of the NKG2D ligand UL16 binding protein-1 (ULBP-1) on dendritic cells. *European Journal of Immunology* **36**, 65-72 (2006).
17. P. Li, D. L. Morris, B. E. Willcox, A. Steinle, T. Spies, R. K. Strong, Complex structure of the activating immunoreceptor NKG2D and its MHC class I-like ligand MICA. *Nat Immunol* **2**, 443-451 (2001).
18. A. Antoun, S. Jobson, M. Cook, C. A. O'Callaghan, P. Moss, D. C. Briggs, Single nucleotide polymorphism analysis of the NKG2D ligand cluster on the long arm of chromosome 6: Extensive polymorphisms and evidence of diversity between human populations. *Human Immunology* **71**, 610-620 (2010).
19. R. A. Eagle, J. A. Traherne, J. R. Hair, I. Jafferji, J. Trowsdale, ULBP6/RAET1L is an additional human NKG2D ligand. *European Journal of Immunology* **39**, 3207-3216 (2009).
20. M. Radosavljevic, B. Ì. t. Cuillerier, M. J. Wilson, O. Clement, S. Wicker, S. Gilfillan, S. Beck, J. Trowsdale, S. Bahram, A Cluster of Ten Novel MHC Class I Related Genes on Human Chromosome 6q24.2-q25.3. *Genomics* **79**, 114-123 (2002).
21. H. A. F. Stephens, MICA and MICB genes: can the enigma of their polymorphism be resolved? *Trends in Immunology* **22**, 378-385 (2001).
22. D. R. Madden, The three-dimensional structure of peptide-MHC complexes. *Annual review of immunology* **13**, 587-622 (1995).
23. D. A. Lawlor, J. Zemmour, P. D. Ennis, P. Parham, Evolution of Class-I MHC Genes and Proteins: From Natural Selection to Thymic Selection. *Annual review of immunology* **8**, 23-63 (1990).
24. R. A. Eagle, J. Trowsdale, Promiscuity and the single receptor: NKG2D. *Nature reviews. Immunology* **7**, 737-744 (2007).
25. A. Antoun, D. Vekaria, R. A. Salama, G. Pratt, S. Jobson, M. Cook, D. Briggs, P. Moss, The genotype of RAET1L (ULBP6), a ligand for human NKG2D (KLRK1), markedly influences

the clinical outcome of allogeneic stem cell transplantation. *British Journal of Haematology* **159**, 589-598 (2012).
26. D. Chen, U. Gyllensten, MICA polymorphism: biology and importance in cancer. *Carcinogenesis* **35**, 2633-2642 (2014).
27. A. McKnight, D. Currie, C. Patterson, A. Maxwell, D. Fogarty, Targeted genome-wide investigation identifies novel SNPs associated with diabetic nephropathy. *The HUGO Journal* **3**, 77-82 (2009).
28. N. Mizuki, M. Ota, M. Kimura, S. Ohno, H. Ando, Y. Katsuyama, M. Yamazaki, K. Watanabe, K. Goto, S. Nakamura, S. Bahram, H. Inoko, Triplet repeat polymorphism in the transmembrane region of the MICA gene: a strong association of six GCT repetitions with Behcet disease. *Proceedings of the National Academy of Sciences of the United States of America* **94**, 1298-1303 (1997).
29. L. Petukhova, M. Duvic, M. Hordinsky, D. Norris, V. Price, Y. Shimomura, H. Kim, P. Singh, A. Lee, W. V. Chen, K. C. Meyer, R. Paus, C. A. B. Jahoda, C. I. Amos, P. K. Gregersen, A. M. Christiano, Genome-wide association study in alopecia areata implicates both innate and adaptive immunity. *Nature* **466**, 113-117 (2010).
30. G. G. Song, J. H. Kim, Y. H. Lee, Associations between the major histocompatibility complex class I chain-related gene A transmembrane (MICA-TM) polymorphism and susceptibility to psoriasis and psoriatic arthritis: a meta-analysis. *Rheumatology international* **34**, 117-123 (2014).
31. A. Isernhagen, D. Malzahn, E. Viktorova, L. Elsner, S. Monecke, F. von Bonin, M. Kilisch, J. M. Wermuth, N. Walther, Y. Balavarca, C. Stahl-Hennig, M. Engelke, L. Walter, H. Bickeböller, D. Kube, G. Wulf, R. Dressel, The MICA-129 dimorphism affects NKG2D signaling and outcome of hematopoietic stem cell transplantation. *EMBO Molecular Medicine* **7**, 1480-1502 (2015).
32. A. Steinle, P. Li, D. L. Morris, V. Groh, L. L. Lanier, R. K. Strong, T. Spies, Interactions of human NKG2D with its ligands MICA, MICB, and homologs of the mouse RAE-1 protein family. *Immunogenetics* **53**, 279-287 (2001).
33. A. Isernhagen, D. Schilling, S. Monecke, P. Shah, L. Elsner, L. Walter, G. Multhoff, R. Dressel, The MICA-129Met/Val dimorphism affects plasma membrane expression and shedding of the NKG2D ligand MICA. *Immunogenetics* **68**, 109-123 (2016).
34. S. Shafi, P. Vantourout, G. Wallace, A. Antoun, R. Vaughan, M. Stanford, A. Hayday, An NKG2D-Mediated Human Lymphoid Stress Surveillance Response with High Interindividual Variation. *Science Translational Medicine* **3**, 113ra124 (2011).
35. D. Jagielska, S. Redler, F. F. Brockschmidt, C. Herold, S. M. Pasternack, N. Garcia Bartels, S. Hanneken, S. Eigelshoven, M. Refke, S. Barth, K. A. Giehl, R. Kruse, G. Lutz, H. Wolff, B. Blaumeiser, M. Bohm, U. Blume-Peytavi, T. Becker, M. M. Nothen, R. C. Betz, Follow-Up Study of the First Genome-Wide Association Scan in Alopecia Areata: IL13 and KIAA0350 as Susceptibility Loci Supported with Genome-Wide Significance. *J Invest Dermatol* **132**, 2192-2197 (2012).
36. J. Hilpert, L. Grosse-Hovest, F. Grunebach, C. Buechele, T. Nuebling, T. Raum, A. Steinle, H. R. Salih, Comprehensive analysis of NKG2D ligand expression and release in leukemia: implications for NKG2D-mediated NK cell responses. *Journal of immunology* **189**, 1360-1371 (2012).
37. P. Vantourout, C. Willcox, A. Turner, C. M. Swanson, Y. Haque, O. Sobolev, A. Grigoriadis, A. Tutt, A. Hayday, Immunological visibility: posttranscriptional regulation of human NKG2D ligands by the EGF receptor pathway. *Sci Transl Med* **6**, 231ra249 (2014).

38. S. Radaev, B. Rostro, A. G. Brooks, M. Colonna, P. D. Sun, Conformational Plasticity Revealed by the Cocrystal Structure of NKG2D and Its Class I MHC-like Ligand ULBP3. *Immunity* **15**, 1039-1049 (2001).
39. R. K. Strong, B. J. McFarland, NKG2D and Related Immunoreceptors. *Advances in protein chemistry* **68**, 281-312 (2004).
40. W. Deng, B. G. Gowen, L. Zhang, L. Wang, S. Lau, A. Iannello, J. Xu, T. L. Rovis, N. Xiong, D. H. Raulet, A shed NKG2D ligand that promotes natural killer cell activation and tumor rejection. *Science*, (2015).
41. D. M. Andrews, M. J. Estcourt, C. E. Andoniou, M. E. Wikstrom, A. Khong, V. Voigt, P. Fleming, H. Tabarias, G. R. Hill, R. G. van der Most, A. A. Scalzo, M. J. Smyth, M. A. Degli-Esposti, Innate immunity defines the capacity of antiviral T cells to limit persistent infection. *The Journal of Experimental Medicine* **207**, 1333-1343 (2010).
42. G. Ferlazzo, M. L. Tsang, L. Moretta, G. Melioli, R. M. Steinman, C. Munz, Human dendritic cells activate resting natural killer (NK) cells and are recognized via the NKp30 receptor by activated NK cells. *J Exp Med* **195**, 343-351 (2002).
43. H. Ghadially, M. Ohana, M. Elboim, R. Gazit, C. Gur, A. Nagler, O. Mandelboim, NK Cell Receptor NKp46 Regulates Graft-versus-Host Disease. *Cell Reports*, (2014).
44. D. Piccioli, S. Sbrana, E. Melandri, N. M. Valiante, Contact-dependent stimulation and inhibition of dendritic cells by natural killer cells. *J Exp Med* **195**, 335-341 (2002).
45. K. Soderquest, T. Walzer, B. Zafirova, L. S. Klavinskis, B. Polic, E. Vivier, G. M. Lord, A. Martin-Fontecha, Cutting edge: CD8+ T cell priming in the absence of NK cells leads to enhanced memory responses. *Journal of immunology* **186**, 3304-3308 (2011).
46. S. N. Waggoner, M. Cornberg, L. K. Selin, R. M. Welsh, Natural killer cells act as rheostats modulating antiviral T cells. *Nature* **481**, 394-398 (2012).
47. A. Gilhar, A. Etzioni, R. Paus, Alopecia areata. *The New England journal of medicine* **366**, 1515-1525 (2012).
48. L. Xing, Z. Dai, A. Jabbari, J. E. Cerise, C. A. Higgins, W. Gong, A. de Jong, S. Harel, G. M. DeStefano, L. Rothman, P. Singh, L. Petukhova, J. Mackay-Wiggan, A. M. Christiano, R. Clynes, Alopecia areata is driven by cytotoxic T lymphocytes and is reversed by JAK inhibition. *Nature medicine* **20**, 1043-1049 (2014).
49. M. Seiler, I. Brabcova, O. Viklicky, P. Hribova, C. Rosenberger, J. Pratschke, A. Lodererova, M. Matz, C. Schonemann, P. Reinke, H. D. Volk, K. Kotsch, Heightened expression of the cytotoxicity receptor NKG2D correlates with acute and chronic nephropathy after kidney transplantation. *American journal of transplantation : official journal of the American Society of Transplantation and the American Society of Transplant Surgeons* **7**, 423-433 (2007).
50. S. Valitutti, S. Muller, M. Salio, A. Lanzavecchia, Degradation of T cell receptor (TCR)-CD3-zeta complexes after antigenic stimulation. *J Exp Med* **185**, 1859-1864 (1997).
51. P. A. van der Merwe, O. Dushek, Mechanisms for T cell receptor triggering. *Nature reviews. Immunology* **11**, 47-55 (2011).
52. S. T. Cox, E. Arrieta-Bolanos, S. Pesoa, C. Vullo, J. A. Madrigal, A. Saudemont, RAET1/ULBP alleles and haplotypes among Kolla South American Indians. *Hum Immunol* **74**, 775-782 (2013).
53. P. Parham, MHC class I molecules and KIRs in human history, health and survival. *Nature reviews. Immunology* **5**, 201-214 (2005).
54. H. D. Kopcow, D. S. Allan, X. Chen, B. Rybalov, M. M. Andzelm, B. Ge, J. L. Strominger, Human decidual NK cells form immature activating synapses and are not cytotoxic.

Proceedings of the National Academy of Sciences of the United States of America **102**, 15563-15568 (2005).
55. M. A. Karimi, J. L. Bryson, L. P. Richman, A. D. Fesnak, T. M. Leichner, A. Satake, R. H. Vonderheide, D. H. Raulet, R. Reshef, T. Kambayashi, NKG2D expression by CD8+ T cells contributes to GVHD and GVT effects in a murine model of allogeneic HSCT. *Blood* **125**, 3655-3663 (2015).
56. B. E. Willcox, G. F. Gao, J. R. Wyer, J. E. Ladbury, J. I. Bell, B. K. Jakobsen, P. A. van der Merwe, TCR Binding to Peptide-MHC Stabilizes a Flexible Recognition Interface. *Immunity* **10**, 357-365 (1999).
57. C. N. Pace, F. Vajdos, L. Fee, G. Grimsley, T. Gray, How to measure and predict the molar absorption coefficient of a protein. *Protein science : a publication of the Protein Society* **4**, 2411-2423 (1995).
58. W. Kabsch, XDS. *Acta Crystallographica Section D* **66**, 125-132 (2010).
59. A. Vagin, A. Teplyakov, Molecular replacement with MOLREP. *Acta Crystallographica Section D* **66**, 22-25 (2010).
60. A. T. Brunger, P. D. Adams, G. M. Clore, W. L. DeLano, P. Gros, R. W. Grosse-Kunstleve, J.-S. Jiang, J. Kuszewski, M. Nilges, N. S. Pannu, R. J. Read, L. M. Rice, T. Simonson, G. L. Warren, Crystallography & NMR System: A New Software Suite for Macromolecular Structure Determination. *Acta Crystallographica Section D* **54**, 905-921 (1998).
61. A. A. Vagin, R. A. Steiner, A. A. Lebedev, L. Potterton, S. McNicholas, F. Long, G. N. Murshudov, REFMAC5 dictionary: organization of prior chemical knowledge and guidelines for its use. *Acta Crystallographica Section D* **60**, 2184-2195 (2004).
62. P. Emsley, K. Cowtan, Coot: model-building tools for molecular graphics. *Acta Crystallographica Section D* **60**, 2126-2132 (2004).
63. R. A. Laskowski, D. S. Moss, J. M. Thornton, Main-chain Bond Lengths and Bond Angles in Protein Structures. *Journal of Molecular Biology* **231**, 1049-1067 (1993).
64. G. J. Kleywegt, T. A. Jones, Detection, delineation, measurement and display of cavities in macromolecular structures. *Acta Crystallographica Section D* **50**, 178-185 (1994).
65. L. A. Kelley, M. J. E. Sternberg, Protein structure prediction on the Web: a case study using the Phyre server. *Nat. Protocols* **4**, 363-371 (2009).
66. L. Li, C. Li, S. Sarkar, J. Zhang, S. Witham, Z. Zhang, L. Wang, N. Smith, M. Petukh, E. Alexov, DelPhi: a comprehensive suite for DelPhi software and associated resources. *BMC Biophysics* **5**, 9-9 (2012).

Acknowledgements: We thank the Birmingham Protein Expression Facility and S. Nicholls for assistance with protein production and purification; the University of Birmingham Macromolecular X-ray Diffraction Facility for assistance with NKG2D data collection; and the Birmingham Clinical Immunology Service and M. Drayson for the provision of primary tumour samples. **Funding:** This research was supported by Bloodwise Programme funding to P.A.H.M. (grant code 12052) and Wellcome Trust New Investigator award funding to B.E.W. (grant code: 099266/Z/12/Z). **Author contributions:** J.Z. and C.R.W. designed and performed in vitro cellular experiments, analyzed data, and wrote the manuscript; F.M. performed structural and protein-protein binding studies, analyzed data, and wrote the manuscript; M.D. designed and performed in vitro γδ stimulation assays; S.H. performed mutagenesis studies and analyzed data; K.K. peformed crystallization studies. A.A. and P.K. performed protein-protein binding assays, RT-PCR, and genotyping; J.C., C.I., and H.P. provided advice and analyzed data; D.B. and R.M. designed the study and provided advice;

and B.E.W. and P.M. supervised the study, designed experiments, analyzed data, and wrote the manuscript. Competing interests: The authors declare that they have no competing interests. **Data and materials availability:** The atomic coordinates and experimental data for the NKG2D-ULBP6 complex structure have been deposited in the RCSB Protein Data Bank (PDB ID: 4S0U).

Fig. 1. Expression of polymorphic variants of *ULBP6.* (**A**) Polymorphisms and haplotypes in the *ULBP6* gene. (**B**) The relative abundances of *ULBP6*, *ULBP2*, and *ULBP5* mRNAs in the indicated cell lines (HCT116 cells were a positive control for *ULBP6* and NKL, LCL, Jurkat, and HeLa cells were negative controls for *ULBP6*) and PBMC-derived immune cell populations were determined by qRT-PCR analysis. Data are shown as mean copy numbers ± SEM of 8 donors. Each symbol represents one donor or cell line, with the differences analyzed by one-way ANOVA with Dunn's multiple comparison post test between indicated groups (*P<0.05) (C) The relative abundance of *ULBP6* mRNA in PBMCs from healthy donors (HDs) and patients with lymphoid malignancies were determined by qRT-PCR analysis. Data are shown as mean ± SEM of 66 patients and 60 HDs. Each symbol represents one patient or HD. Statistical differences were analyzed by Mann-Whitney test. ****P < 0.0001. (**D**) The relative abundances of *ULBP2*, *ULBP5*, and *ULBP6* mRNAs in primary B cells from healthy donors and CLL patients were determined by qRT-PCR analysis. Data are shown as mean ± SEM of 8 HDs and 13 CLL patients. Each symbol represents one HD or CLL patients. Statistical differences were determined by Mann-Whitney test. *P < 0.05. (**E**) The relative cell surface abundance of ULBP2, ULBP5, and ULBP6 on B cells from one representative healthy donor (gated on $CD19^+$ cells) and one representative CLL patient (gated on $CD19^+CD5^+$ tumor cells) were determined by flow cytometric analysis. Staining with the isotype control is shaded. Data are representative of four independent experiments. (**F**) The mean fluorescence intensity (MFI) values of cell surface ULBP2, ULBP5, and ULBP6 staining on healthy B cells (n = 3 donors) and CLL cells (n = 4 patients) were 1.4-fold and 1.8-fold the MFI of isotype control, respectively. Statistical differences between the

MFIs of healthy donor B cells and CLL cells were determined by Mann-Whitney test. *P < 0.05. (**G**) The relative abundance of *ULBP6* mRNA in PBMCs from *0602*-negative (n = 39) versus *0602*-positive (n = 45) patients (left) and in 0*601*-positive (n = 57) versus *0601*-negative (n = 27) patients (right). Data are shown as mean ± SEM. Each symbol represents one patient. Statistical differences were determined by Mann-Whitney test; ns, not significant.

Fig. 2. SPR analysis of NKG2D-ULBP interactions. (**A**) Specific binding of NKG2D to ULBP0601, ULBP0602, and ULBP1, in comparison to Endothelial Protein C Receptor control. Recombinant NKG2D was expressed in *E. coli* and ULBP proteins were expressed in the *Drosophila* expression system. (**B**) Equilibrium affinity analysis of NKG2D interactions with ULBP0601, ULBP0602, and ULBP1. Data from a representative experiment are shown. Equilibrium affinity measurements injecting ULBP0601 or ULBP0602 over immobilized NKG2D yielded Kd values similar to those obtained from experiments performed with the opposite orientation [136.5 nM +/-10.6 for ULBP0601 (n = 8); 11.2 nM +/-0.6 for ULBP0602 (n = 4)]. The number of independent equilibrium binding analyses performed for ULBP0601, ULBP0602, and ULBP1 were 14, 10, and 8, respectively. (**C**) Kinetic analysis of the dissociation of NKG2D from ULBP0601, ULBP0602, and ULBP1. Data were collected at a flow rate of 50 µl/min to minimize mass transport effects. Dissociation data were normalized to assist comparison [ULBP0602 (n = 6): k_{off} ~0.00125s^{-1}, $t_{1/2}$ ~550 seconds; ULBP0601 (n = 6): k_{off} = 0.022s^{-1}, $t_{1/2}$ ~31 s; ULBP1 (n = 6): k_{off} ~0.030s^{-1}, $t_{1/2}$ ~23 s].

Fig. 3. Structural features of the NKG2D-ULBP0602 complex. (**A**) NKG2D homodimer [NKG2D-A (pale green) and NKG2D-B (salmon)] interacting with monomeric ULBP0602 (cyan). Recombinant NKG2D and ULBP0602 were expressed in *E. coli.* NKG2D regions that

stabilize the complex interface include loop 1 (L1), the β5'-β5 loop (stirrup loop), and strand β6. Secondary structural elements are highlighted. (**B**) Stereoview of the 2.4 Å-resolution composite omit the 2*Fo-Fc* electron density map for the ULBP0602 α1 helix (residues 99DILTEQLL106) contoured at 1.5σ (black). (**C**) Structural comparison of ULBP0602 (cyan) and ULBP3 (light orange, PDB code: 1KCG). Structural differences are highlighted with black dashed circles. (**D**) Narrow MHC-like antigen-binding groove of ULBP0602 is lined with bulky side-chains (shown in stick format), which prevent peptide binding. (**E**) Top view of the complex from the perspective of NKG2D. The receptor-ligand interaction conforms to the diagonal mode of docking, with footprints for NKG2D-A and NKG2D-B shown in light green and salmon, respectively.

Fig. 4. Stabilization of the NKG2D-ULBP0602 complex interface. (**A**) Stabilization of the NKG2D-ULBP0602 complex. The interface is dominated by hydrogen bonding interactions (black dashed lines) mediated by polar residues (shown in stick format). The color coding is the same as that used in Fig. 3A. (**B**) Comparison of the molecular surface electrostatic potential for ULBP6, ULBP3 (PDB ID: 1KCG), MICB (PDB ID: 1JE6), MICA (PDB ID: 1B3J), and Phyre-derived models of ULBP1, 2, 4, and 5, calculated with Delphi. There is a conserved electronegative patch (residues labelled) that may facilitate the docking of NKG2D in the diagonal orientation. The potential scale ranges from -7 (red) to +7 (blue) in units of kT/e. (**C**) The NKG2D-ULBP0602 complex interface is stabilized by nonpolar residues (shown in stick format) that combine to form two distinct hydrophobic patches (A and B). The color coding is the same as that used in Fig. 3A. (**D**) Structure of the NKG2D-ULBP0602 complex showing the location of *ULBP6* polymorphic residues at positions 106 and 147 (stick format, yellow). (**E**) Molecular surface electrostatic potential for ULBP0602. Leu^{106} in ULBP0602 inserts directly into the hydrophobic pocket of patch B of NKG2D,

forming extensive hydrophobic contacts with surrounding residues. (**F**) Predicted molecular surface electrostatic potential for ULBP0601. Introduction of Arg^{106} in ULBP0601 is likely to be detrimental for NKG2D binding. (**G**) Specific binding (left) and equilibrium affinity analysis (right) of the interaction of NKG2D with wild-type ULBP0602 (n = 2) and wild-type ULBP0601 (n = 2), and with ULBP0602 bearing point mutations at positions 106 (n = 2) and 147 (n = 2).

Fig. 5. Compared to ULBP0602, ULBP0601 elicits enhanced NK cell–mediated killing of targets. (**A**) Validation of the equivalent cell surface expression of the indicated allotypes by different CHO cell lines. CHO-parental (shaded histogram), CHO-ULBP0601 (solid line), and CHO-ULBP0602 (dotted line) cells were stained with antibody against ULBP2/5/6 and then were analyzed by flow cytometry. Data are representative of four independent experiments. (**B**) Assay of the specific cytotoxic responses of PBMCs from a healthy donor to CHO cells expressing ULBP0601 or ULBP0602 in the presence (right panels) or absence (including control antibody, middle panels) of blocking anti-NKG2D antibody. Data are representative of four independent experiments. (**C**) Left: Comparison of the magnitude of specific cytotoxic responses of cells from 18 healthy donors to ULBP0601- or ULBP0602-expressing CHO, depicted in increasing magnitude of absolute response. Each symbol represents one healthy donor. Right: Representation in boxplots. Data are shown as means and the full range. Differences between ULBP0601 and ULBP0602 were analyzed by Wilcoxon matched-pairs signed rank test. $^{**}P < 0.01$. (**D**) The percentages of NK cells expressing the degranulation marker CD107a were measured after activation in response to ULBP0601- or ULBP0602-expressing CHO cells. Data are representative of three independent experiments from three healthy donors (HD1 to HD3). Left: Data are means ± SEM. Right: Boxplots. The data are shown as means and the full range. Differences between

ULBP0601 and ULBP0602 were analyzed by Wilcoxon matched-pairs signed rank test. *P < 0.05.

Fig. 6. Soluble ULBP0602 blocks the binding of anti-NKG2D antibody and inhibits the activation of NK cells. (**A**) NKL cells were incubated with PBS (solid line) or 10 μg /ml of soluble ULBP0601 (dotted line) or ULBP0602 (dashed line) for 16 hours before NKG2D surface expression was analyzed by flow cytometry. The filled gray histogram represents isotype control staining. Data are representative of three independent experiments. (**B**) NKL cells were incubated with the indicated concentrations of soluble ULBP0601 or ULBP0602. NKG2D surface staining was analyzed by flow cytometry and quantified and the differences were analyzed by two-way ANOVA with Bonferroni-corrected post-hoc comparisons between the indicated groups. ***$\underline{P}$ < 0.001. Data are means ± SEM from three independent experiments. (**C**) Primary NK cells from 6 donors were co-cultured with K562 cells with or without soluble ULBP0601 or ULBP0602 (10 μg /ml), and NK cell activation was quantified by the flow cytometric analysis of CD107a staining. The differences between the indicated groups were analyzed by one-way ANOVA with Turkey's multiple comparison post test. **P < 0.01, ***P < 0.001. (**D**) The concentration of soluble ULBP6 released during the culture of CHO-ULBP0601 and CHO-ULBP0602 cells was quantified by ELISA. Data are means ± SEM from three independent experiments. (**E**) NKL cells were cultured with the conditioned medium from the indicated cells and then were stained with ULBP2-Fc proteins followed by APC-conjugated anti-human Fc and flow cytometric analysis. Data are means ± SEM from three independent experiments. Differences were analyzed by Mann-Whitney test. *P < 0.05, **P < 0.01.

Fig. 7. Compared to ULBP0602, ULBP0601 elicits enhanced T cell–mediated killing of targets. (**A**) NKG2D and TCR Vδ2 expression on 14-day expanded peripheral blood γδ T-cells. Flow cytometry plots are representative of three independent experiments from three different donors. (**B**) Parental (blue) and ULBP0601- or ULBP06020-expressing (red) CHO cells were co-cultured with or without expanded peripheral blood γδ T-cells at an effector-to-target (E:T) ratio of 10:1 in medium or HMB-PP/IL-2. The CHO cell lines were then assessed for specific cell death. (**C**) Parental, ULBP0601-, and ULBP0602-expressing CHO cells were co-cultured with γδ T-cells and HMB-PP/IL-2 at the indicated E:T ratios for 18 hours. Representative flow cytometry plots (B) and graphs showing mean ± SEM specific killing of CHO cells (C) are from three independent experiments with five different donors. Differences between the ULBP0601- and ULBP0602-expressing cells were analyzed by two-way ANOVA with Bonferroni-corrected post-hoc comparisons between the indicated groups. **P* < 0.05, ****P* < 0.001. (**D**) Validation of cell surface NKG2D expression on EBV-specific CTLs. Data are representative of three independent experiments. (**E**) Validation of the equivalent cell surface expression of ULBP0601 (solid line) and ULBP0602 (dashed line) relative to untransfected Jurkat cells (dotted line) and isotype control staining (shaded histogram). Cells were stained with anti-ULBP2/5/6 antibody. Data are representative of three independent experiments. (**F**) Analysis of the production of IFN-γ by EBV-specific CTLs in response to ULBP0601- or ULBP0602-expressing Jurkat cells pulsed with cognate peptide antigen. Data are means ± SEM from three independent experiments. Differences between the ULBP0601 and ULBP0602 cells were analyzed by two-way ANOVA with Bonferroni-corrected post-hoc comparisons. **P* < 0.05, ***P* < 0.01, *****P* < 0.0001.

Fig. 8 *ULBP6* polymorphism at residue 106 affects effector cell functions through alterations in NKG2D-mediated signaling. (**A**) Validation of the cell surface expression of

NKG2D on the NKL cell line. NKL cells were stained with anti-NKG2D antibody. Histograms show NKG2D cell surface expression on NKL cells (solid line) compared to isotype control staining (shaded histogram). Data are representative of three independent experiments. (**B**) Analysis of the NKL cell–mediated killing of ULBP0601- and ULBP0602-expressing cells. Differences between the indicated groups were analyzed by two-way ANOVA with Bonferroni-corrected post-hoc comparisons. *P < 0.05, **P < 0.01, ***P < 0.001, ****P < 0.0001. Data are means ± SEM from three independent experiments. (**C**) Analysis of the cell surface expression of ULBP0602-L106R (long dash), ULBP0602-T147I (short dash), ULBP0602 (dotted line), and ULBP0601 (solid line) in comparison to parental CHO cells (shaded histogram). All cells were stained with anti-ULBP2/5/6 antibody. Data are representative of three independent experiments. (**D**) Cytotoxic response elicited by transfected CHO cells expressing the indicated WT and mutant ULBP6 forms. Data are means ± SEM from three independent experiments. Differences were analyzed by Mann-Whitney test. *P < 0.05, **P < 0.01. (**E**) Differential killing and binding affinity of WT ULBP0601 (n = 2; Kd = 148.2 +/- 1.2 nM), WT ULBP0602 (n = 2, Kd = 13.4 +/- 0.2 nM), ULBP0602-L106R (n = 2, Kd = 148.3 +/- 0.4 nM), and ULBP0602-T147I (n = 2, Kd = 13.4 +/- 0.1 nM). (**F**) Analysis of the extent of NKG2D downregulation elicited by ULBP0601 and ULBP0602. Differences between the indicated groups were analyzed by two-way ANOVA with Bonferroni-corrected post-hoc comparisons. **P < 0.01, ****P < 0.0001. Data are means ± SEM from three independent experiments. (**G**) Calcium flux analysis of NKL cells in response to NKG2D-ULBP6 interactions. Data are the relative MFI of the NKL cells after the addition of the indicated CHO-ULBP6 cells compared to the basal MFI of the NKL cells and are shown as means ± SEM from three independent experiments. Differences between ULBP0601 and ULBP0602 were analyzed by Mann-Whitney test. *P < 0.05.

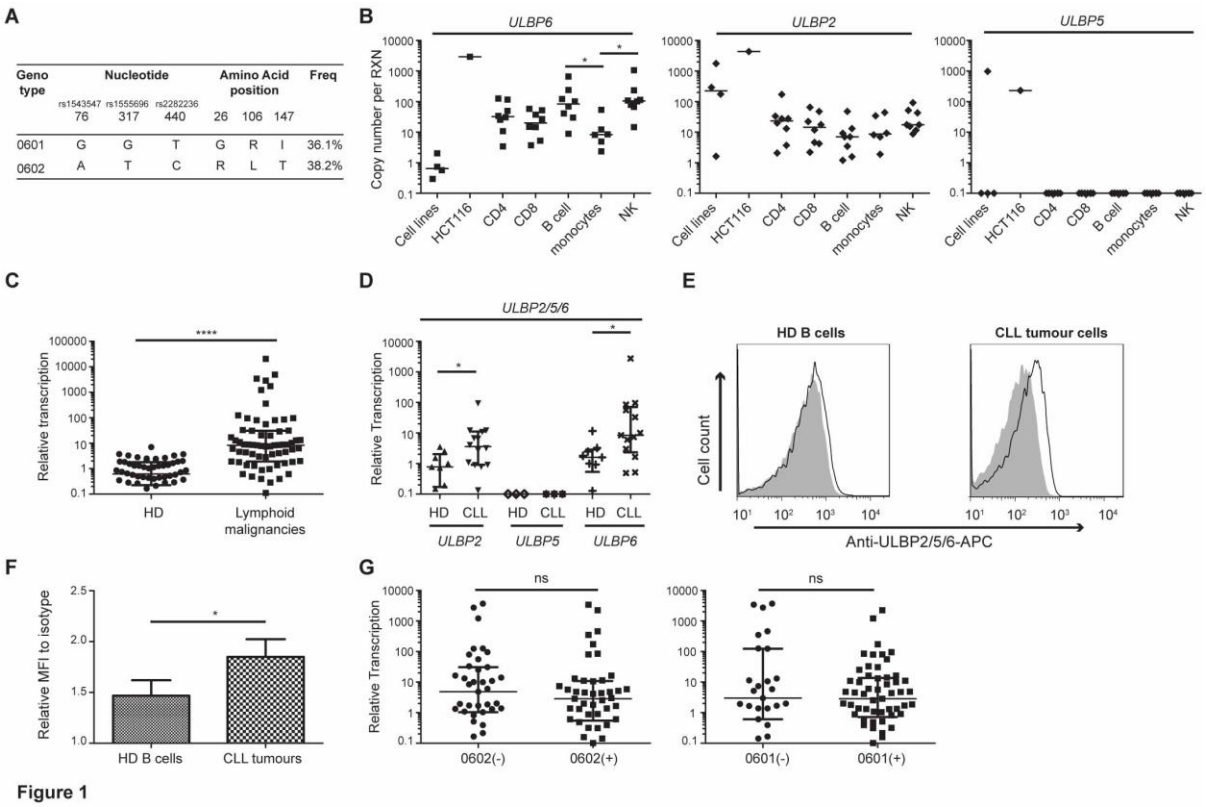

Figure 1

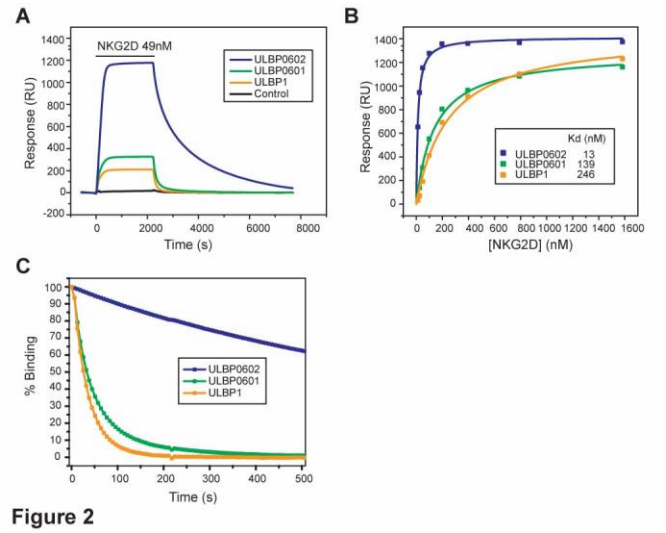

Figure 2

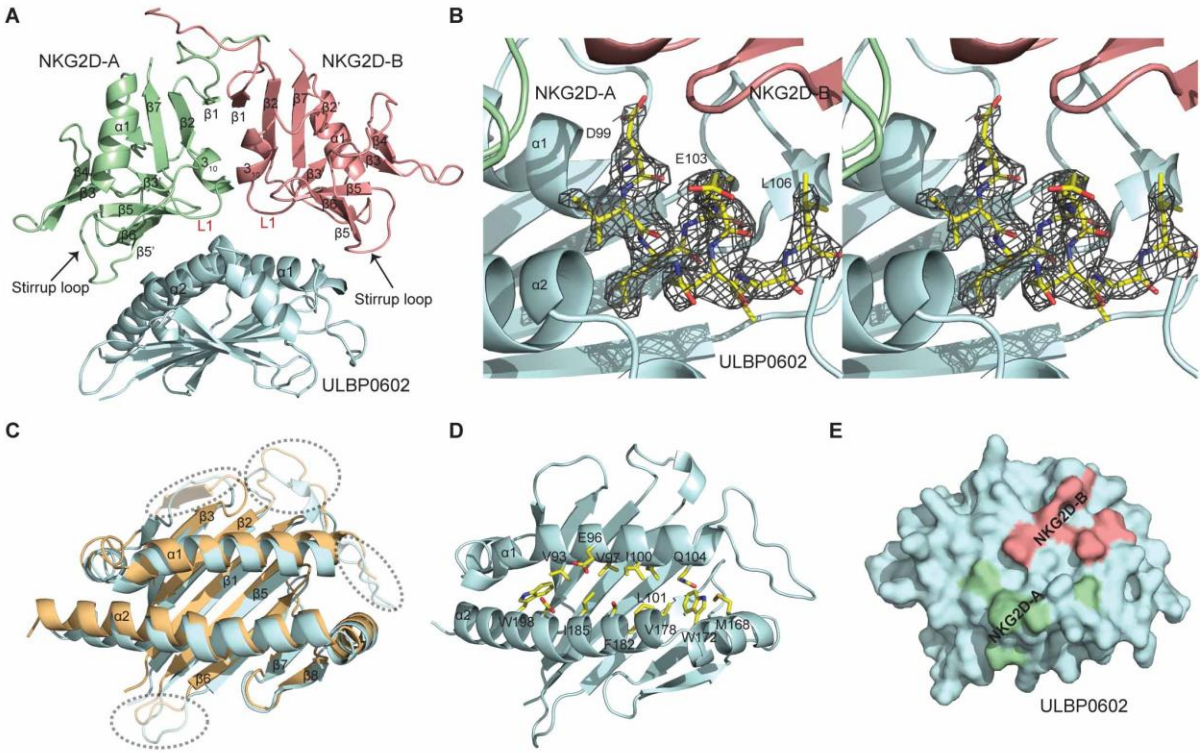

Figure 3

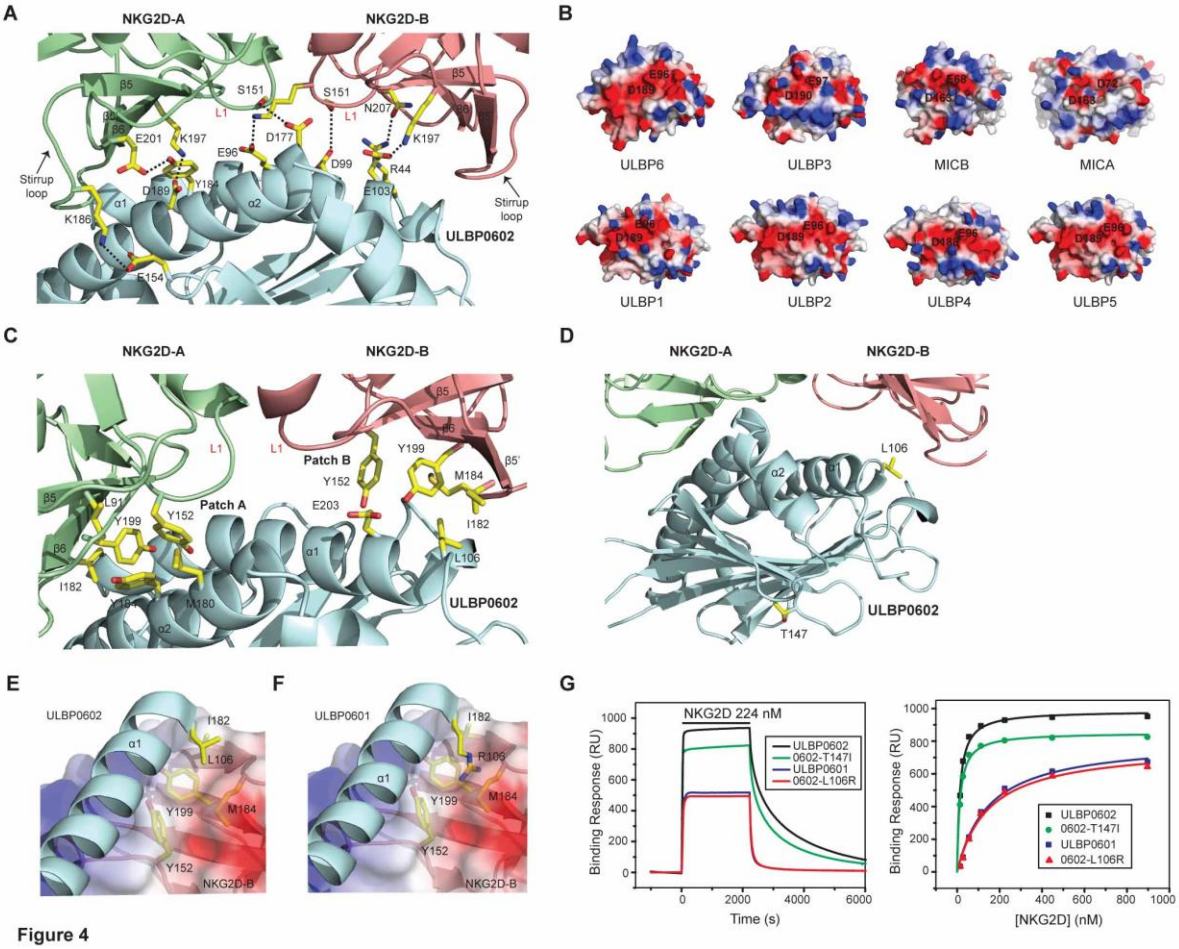

Figure 4

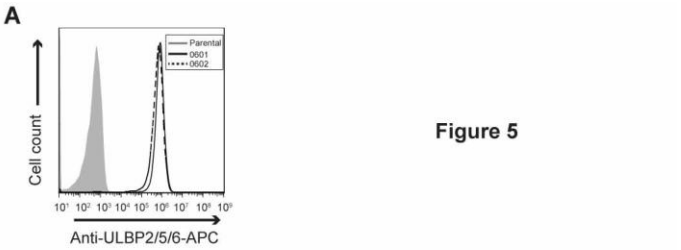

Figure 5

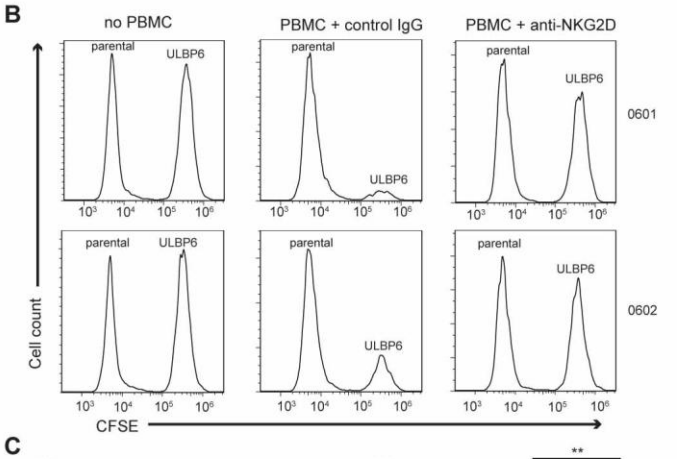

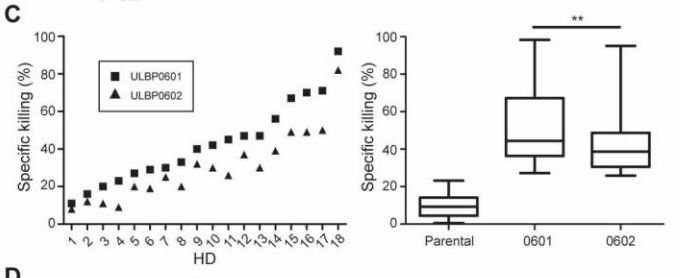

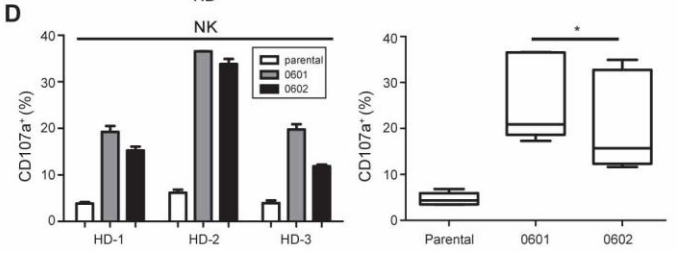

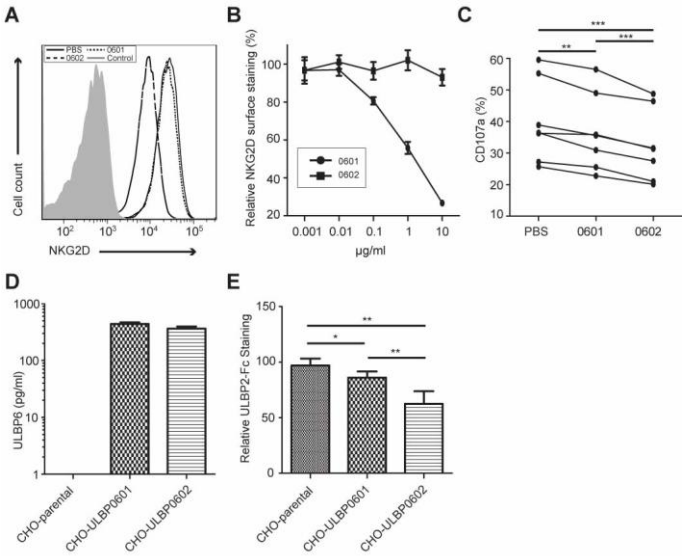

Figure 6

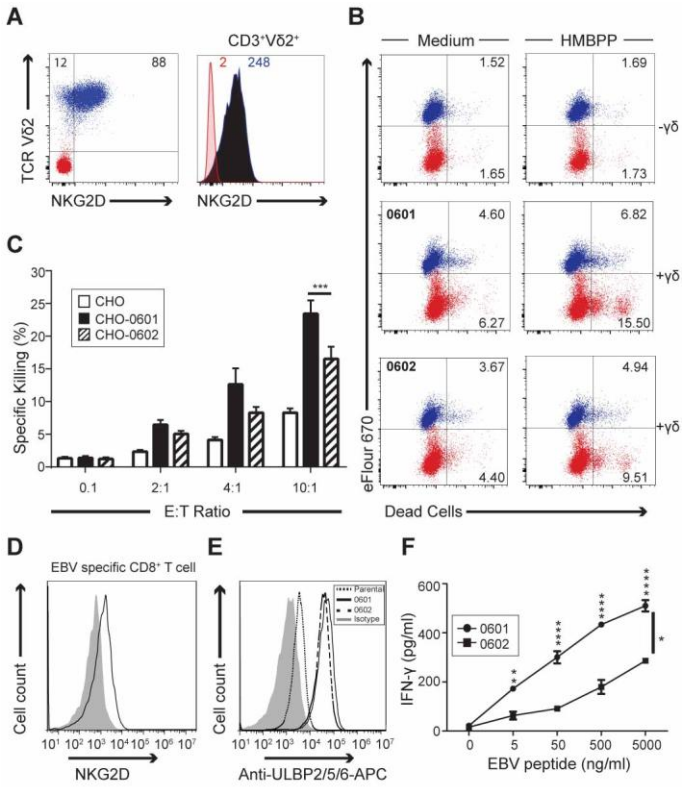

Figure 7

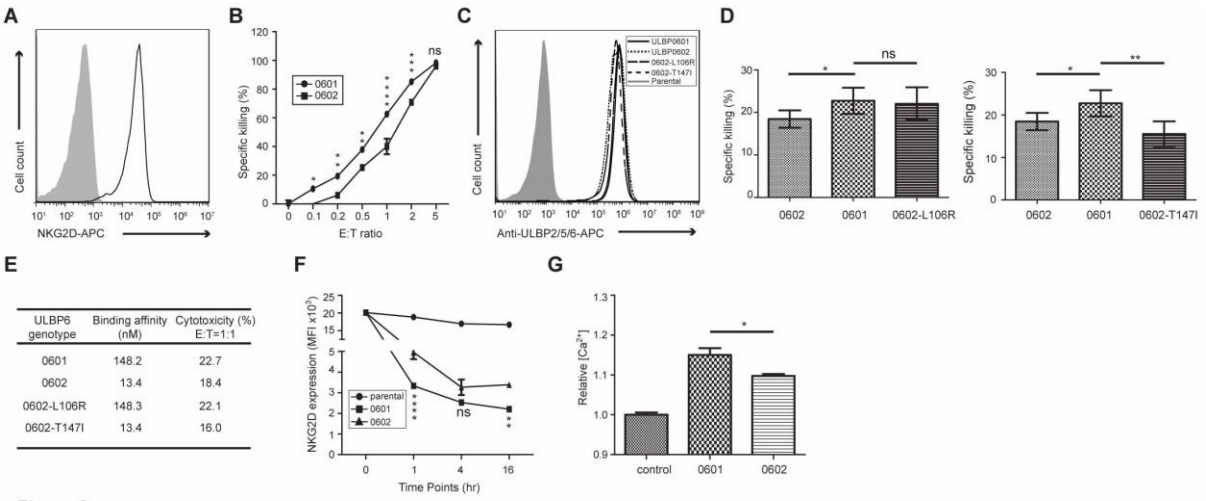

ULBP6 genotype	Binding affinity (nM)	Cytotoxicity (%) E:T=1:1
0601	148.2	22.7
0602	13.4	18.4
0602-L106R	148.3	22.1
0602-T147I	13.4	16.0

Figure 8